Development 138, 4475-4485 (2011) doi:10.1242/dev.061952

MIG-15 and ERM-1 promote growth cone directional migration in parallel to UNC-116 and WVE-1

Jérôme Teulière[1,2,*], Christelle Gally[1], Gian Garriga[2], Michel Labouesse[1,*] and Elisabeth Georges-Labouesse[1]

SUMMARY

Neurons require precise targeting of their axons to form a connected network and a functional nervous system. Although many guidance receptors have been identified, much less is known about how these receptors signal to direct growth cone migration. We used *Caenorhabditis elegans* motoneurons to study growth cone directional migration in response to a repellent UNC-6 (netrin homolog) guidance cue. The evolutionarily conserved kinase MIG-15 [homolog of Nck-interacting kinase (NIK)] regulates motoneuron UNC-6-dependent repulsion through unknown mechanisms. Using genetics and live imaging techniques, we show that motoneuron commissural axon morphology defects in *mig-15* mutants result from impaired growth cone motility and subsequent failure to migrate across longitudinal obstacles or retract extra processes. To identify new genes acting with *mig-15*, we screened for genetic enhancers of the *mig-15* commissural phenotype and identified the ezrin/radixin/moesin ortholog ERM-1, the kinesin-1 motor UNC-116 and the actin regulator WVE-1 complex. Genetic analysis indicates that *mig-15* and *erm-1* act in the same genetic pathway to regulate growth cone migration and that this pathway functions in parallel to the UNC-116/WVE-1 pathway. Further, time-lapse imaging of growth cones in mutants suggests that UNC-116 might be required to stimulate protrusive activity at the leading edge, whereas MIG-15 and ERM-1 maintain low activity at the rear edge. Together, these results support a model in which the MIG-15 kinase and the UNC-116–WVE-1 complex act on opposite sides of the growth cone to promote robust directional migration.

KEY WORDS: Nck-interacting kinase (NIK), Moesin, Kinesin-1, WAVE, Growth cone directional migration, *Caenorhabditis elegans*

INTRODUCTION

During nervous system development, guidance cues regulate cell and growth cone migration to ensure precise neuronal connectivity to distant targets. These signals are transduced by transmembrane receptor proteins, which subsequently remodel the growth cone cytoskeleton and change its motility. Although numerous genes regulating neurite outgrowth have been discovered, the specific cellular processes they regulate in vivo are not clearly understood (Hatten, 2002; Chilton, 2006; Silhankova and Korswagen, 2007; Quinn and Wadsworth, 2008).

In the nematode *Caenorhabditis elegans*, neurite outgrowth has been precisely described using time-lapse imaging of developing D-type GABAergic (γ-aminobutyric acid-secreting) motoneurons (Fig. 1A) (Knobel et al., 1999). The six DD and 13 VD neurons send a commissural axonal process during embryogenesis (DDs) or larval development (VDs). Commissures run from the ventral nerve cord (VNC) towards the dorsal nerve cord (DNC) (Sulston and Horvitz, 1977; Sulston et al., 1983; Knobel et al., 1999). Dorsalward directional migration depends on the ventral repellent netrin homolog UNC-6 signal and its receptors UNC-5 and UNC-40 (McIntire et al., 1992; Ishii et al., 1992; Hamelin et al., 1993; Chan et al., 1996; Keleman and Dickson, 2001; Quinn and Wadsworth, 2008).

We previously identified *mig-15* as a gene necessary for VD and DD axon outgrowth in *C. elegans* (Poinat et al., 2002). *mig-15* encodes the ortholog of the mouse Nck-interacting kinase (NIK) and of *Drosophila melanogaster* Misshapen (Msn). MIG-15, NIK and Msn belong to the Ste20 germinal center kinase (GCK) IV protein family of serine threonine kinases or mitogen-activated protein kinase kinase kinase kinase 4 (MAP4K4). Little is known about the cellular functions and targets of MAP4K4 kinases in vivo, except that they can activate intracellular signaling cascades such as the c-Jun N-terminal kinase (JNK) pathway (Su et al., 1998; Dan et al., 2001; Machida et al., 2004). Genetic data in different model systems indicate that MAP4K4 kinases are necessary for cell polarity and directional cell and growth cone migrations. In *Drosophila*, Msn is required for epithelial planar cell polarity and embryonic dorsal closure in gastrulating embryos (Su et al., 1998; Paricio et al., 1999). In vertebrates, the zebrafish Msn is needed for epithelial morphogenesis during gastrulation, whereas *Nik*$^{-/-}$ mouse embryos have gastrulation defects and die from migration defects of mesodermal and endodermal cells (Xue et al., 2001; Köppen et al., 2006). In *C. elegans*, MIG-15 regulates Q neuroblast polarity and migration (Chapman et al., 2008); it acts possibly downstream of Rac GTPases for postdeirid neuron (PDE) axon outgrowth (Shakir et al., 2006).

Here, we show that *mig-15* functions cell-autonomously during VD commissure outgrowth. We establish that *mig-15* commissural defects result from abnormal growth cone polarity and a failure to cross longitudinal obstacles. To identify genes acting together with *mig-15* to promote growth cone migration, we screened for genetic enhancers of the *mig-15* VD/DD commissural phenotype. By combining genetic analysis with time-lapse imaging of growth cones, we could identify one gene acting in the same pathway as *mig-15* to restrict protrusive activity to the distal half of the growth cone, and another group of genes acting in parallel to stimulate distal protrusive activity. We also suggest that *mig-15* acts in the same pathway as *unc-5* to polarize the growth cone in response to the UNC-6 attractive signal. We discuss a model for MIG-15 activity based on these data.

[1]IGBMC, CNRS/Université de Strasbourg UMR7104, INSERM U964, 1 rue Laurent Fries, BP10142, Illkirch, 67400 France. [2]Department of Molecular and Cell Biology, Helen Wills Neuroscience Institute, University of California Berkeley, Berkeley, CA 94720, USA.

*Authors for correspondence (jteuliere@berkeley.edu; lmichel@igbmc.fr)

Accepted 8 August 2011

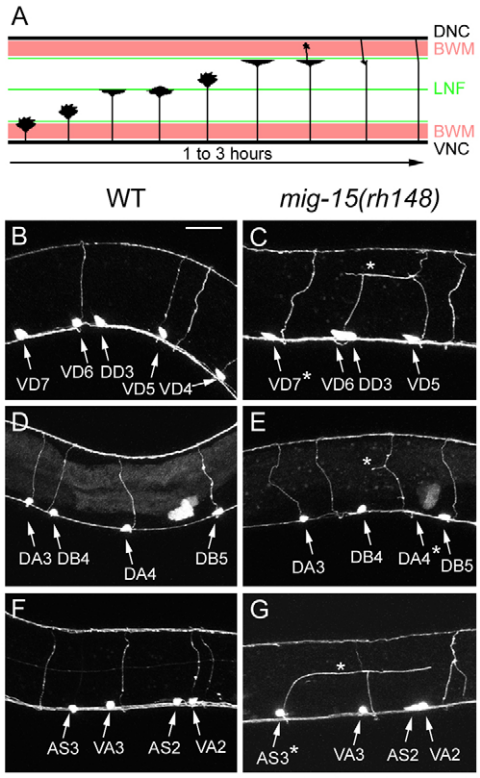

Fig. 1. Commissural defects in *mig-15 C. elegans* mutants. (**A**) VD neuron axonal outgrowth. In late L1 larvae, rapid migration of VD growth cones from the ventral nerve cord (VNC) towards the dorsal nerve cord (DNC) leads to the formation of commissures along a dorsally directed circumferential path. Migration stalls when the growth cone encounters obstacles, such as longitudinal nerve fascicles (LNF) or body wall muscles (BWM), and eventually resumes upon growth cone reorganization to form a large lamellipodia and/or cytoplasmic fingers to cross the obstacle (Knobel et al., 1999). (**B-G**) Representative commissures of (B,C) the VD/DD GABAergic, (D,E) the DA/DB cholinergic, and (F,G) the VA/AS cholinergic neurons from wild-type (B,D,F) and *mig-15(rh148)* (C,E,G) L4 larvae. Asterisks indicate defective commissures and corresponding cell bodies; arrows indicate cell bodies. Dorsal side is up, anterior is to the right (B,C,F,G) or to the left (D,E). Scale bar: 25 μm.

MATERIALS AND METHODS

C. elegans genetics

Nematodes were cultured as described (Brenner, 1974). N2 Bristol was used as the wild-type strain and all experiments were performed at 20°C.

Mutations and integrated arrays used in this study:

LG I: *let-502(sb118ts)*, *erm-1(tm677)*, *tba-1(or346ts)*, *zdIs5[Pmec-4::gfp]*, *hT2 I, III*.

LG II: *unc-104(e1265)*, *cdc-42(gk388)*, *rrf-3(pk1426)*, *juIs76[Punc-25::gfp]*, *krIs6[Punc-47::DsRed2]* (a gift from Dr J. L. Bessereau, ENS Paris, France), *mIn1*.

LG III: *unc-116(e2310)*, *unc-16(e109, ju146, n730)*.

LG IV: *kgb-1(um3)*, *eri-1(mg366)*, *unc-33(e204)*, *kgb-2(gk361)*, *unc-5(e53, e152)*, *bicd-1(ok2731)*, *jnk-1(gk7)*, *evIs82b[Punc-129::gfp]*, *nT1 IV, V*.

LG V: *gmIs65[sra-6P::mcherry; tph-1P::gfp]* (a gift from Dr R. Ikegami, Berkeley, USA).

LG X: *jkk-1(km2)*, *mek-1(ks54)*, *sek-1(km4)*, *mig-15(rh80, rh148, rh326)*, *oxIs12[Punc-47::gfp; lin-15+]*.

Unmapped: *evIs111[F25B3.3::GFP]*; *gmIs80[Punc-30::ΔNerm-1::gfp, 100 ng/μl; Pmyo-2::mcherry, 3 ng/μl]* (spontaneous integration; this study).

Unless otherwise stated, the description of mutants and integrated transgenes is available at Wormbase (http://www.wormbase.org).

DNA manipulations and extra-chromosomal arrays

To label the body wall muscles, the mCherry cDNA was amplified from *pcc1::mcherry* (pHD246, a gift from Dr H. Fares, University of Arizona, USA) and cloned into pPD95.86 (Addgene, Cambridge, USA) using *Nhe*I and *Kpn*I to generate *Pmyo-3::mcherry*.

For *mig-15* rescue and overexpression experiments, the *mig-15* unspliced coding sequence was cloned behind the GABAergic neuron-specific *unc-25* promoter in pSC325 (Jin et al., 1999; Poinat et al., 2002).

For *erm-1* cell-specific RNAi, the *erm-1* cDNA (a gift from O. Bossinger, RWTH, Aachen University, Germany) was cloned in forward and reverse orientations in pSC325 at the *Kpn*I site to obtain the *Punc-25::erm-1 forward* and *Punc-25::erm-1 reverse* plasmids. Linear 3 kb DNA fragments comprising the *unc-25* promoter fused to the *erm-1* cDNA in both orientations were obtained by digesting both plasmids with *Cla*I, *Eag*I and *Sca*I.

A constitutively active ERM-1(T544D) construct was created by PCR fusion mutagenesis of an *erm-1* cDNA, then cloned into pSC325 using *Kpn*I [*Punc-25::erm-1(T544D)* plasmid]. A control *Punc-25::erm-1* plasmid was generated in parallel.

For ΔNERM-1::GFP expression, a PCR-generated *erm-1::gfp* fragment was first cloned downstream of the *unc-30* promoter obtained from pSC157 (kindly provided by Y. Jin, UCSD, La Jolla, USA) using MultiSite Gateway cloning (Invitrogen). An in-frame 1128-nucleotide deletion encoding the N-terminal FERM domain was created by *Ban*II digestion of *Punc-30::erm-1::gfp*.

All extra-chromosomal arrays used in this study are described in Table 1.

Axon defect analysis

Scoring was performed using a DMRB epifluorescence microscope (Leica Microsystems) equipped with a Plan APO 100× 1.4 objective. The *oxIs12*, *juIs76* and *krIs6* markers were used to label the VD/DD neurons. The *bgEx21* and *evIs82b* markers were used to label the VA/AS and DA/DB neurons, respectively. The pan-neuronal *evIs111* and the body wall muscle *mcEx491* markers were used to define landmarks along the ventral-dorsal migration path of VD/DD commissural axons. Longitudinal fascicles were grouped by ventral-dorsal position on the right side of the animals. VD/DD defects were scored in *oxIs12* animals on both sides in L4 larvae, on the right side only in L2 larvae. Classes of defects I, II and III (see Results) were scored independently for each commissure. Class II and III defects were not scored on arrested class I commissures. The occasional neurons the cell body of which was not in the VNC were not scored. The *gmIs65* and the *zdIs5* markers were used to label the HSN of young adults and the touch neurons A/PVM of L4 larvae, respectively, and defects were scored on the top sides.

RNAi by feeding

RNAi-sensitizing mutations *eri-1(mg366)* and *rrf-3(pk1426)* (Kennedy et al., 2004; Simmer et al., 2003) were introduced into wild-type, *mig-15(rh148)* and *unc-116(e2310)* animals carrying the *oxIs12* marker. Worm feeding was performed as described (Timmons et al., 2001). In control experiments, GFP downregulation was observed in up to 65% of the worms.

Candidate *mig-15* enhancers were genes encoding proteins with actin- and microtubule-binding domains, axon guidance regulators, predicted genetic interactors of *mig-15* and *ina-1* or *pat-3* (Zhong and Sternberg, 2006), as well as known signaling partners of MAP4K4 in other systems. A few candidate genes were directly tested by mutations. See Table S1 in the supplementary material for a list of primers for all genes tested. RNAi clones were recovered from the Ahringer bacterial library (Kamath et al., 2003), sequenced and retransformed into fresh HT115(DE3) cells, except the *unc-34* clone constructed as described (Fleming et al., 2010). Commissures were examined in at least 20 animals per candidate enhancer. Enhancers were classified as weak [twice as many commissural defects as in *mig-15(rh148)*] or strong (more than twice as many). For each positive hit, RNAi was performed in *mig-15(+)* animals to determine whether the enhancement was *mig-15* dependent. The enhancer screen was performed twice and the clones reproducibly enhancing the *mig-15(rh148)* phenotype were considered to be positive hits.

Table 1. Extra-chromosomal arrays used

Name	Construct	Concentration (ng/μl)	Marker	Reference
bgEx21	*Punc-53::GFP*	–	*rol-6(su1006)*	(Stringham et al., 2002)
kyEx926	*Punc-86::mig-10::YFP*	–	*Podr-1::DsRed*	(Adler et al., 2006)
mcEx491	*Pmyo-3::mCherry*	50	–	This study
gmEx545 gmEx546	*Punc-25::mig-15 unspliced*	10	*Pmyo-2::gfp*	This study
gmEx552	*Punc-25::mig-15 unspliced*	100	*Pmyo-2::gfp*	This study
mcEx505 mcEx506	*Punc-25::unc-16*	50	*Pmyo-2::gfp*	This study
mcEx516 mcEx517	*Pmyo-3::unc-16*	50	*Pmyo-2::gfp*	This study
gmEx560	*Punc-25::erm-1 cDNA forward + reverse*	2.5	*Pmyo-2::mcherry*	This study
mcEx473 mcEx474	*Punc-25::erm-1 T544D*	50	*Pmyo-2::GFP*	This study
gmEx570 gmEx571	*Punc-25::erm-1*	50	*Pmyo-2::GFP*	This study
gmEx593 gmEx595	*Punc-86::mig-15 unspliced*	10	*Pmyo-2::GFP*	This study

Live imaging

We used a Leica TCS SP5 fast confocal system with Argon and DPSS 561 lasers on a DMI6000 microscope (Leica Microsystems) equipped with HCX Plan Apo 63× 1.4 and 40× 1.25 objectives, to image growth cones and commissures, respectively.

Synchronized arrested L1 larvae were transferred on OP50 bacteria for 16-20 hours, depending on the genotype, before imaging VD growth cones. Larvae were anesthetized with 1 mM levamisole in M9 solution and mounted as described (Knobel et al., 1999). High molecular weight (>300 kDa, Sigma) poly-L-lysine-coated coverslips were used to reduce worm movements. Time-lapse movies were obtained by acquiring stacks of 15 images with a *z*-step size of 0.5 μm every minute. Maximum intensity projections were adjusted for contrast and brightness and a Gaussian blur filter of 0.9 μm was applied using ImageJ software. Growth cone movies were realigned using the StackReg plugin for ImageJ (http://bigwww.epfl.ch/thevenaz/stackreg/).

Protrusive activity was quantified in growth cones actively migrating between the ventral and dorsal body wall muscles. Each binarized frame was subtracted from the previous using the DeltaF ImageJ plugin (http://www.macbiophotonics.ca/imagej/t.htm#t_deltaF). Protrusions were then identified and manually counted in the distal and proximal halves of the growth cones in movies ranging from 25 to 75 minutes (see Movie 13 in the supplementary material).

For MIG-10::YFP imaging in HSN, 15 images per *z*-stack were acquired with the 488 nm ray of a Marianas spinning disc confocal microscope (Intelligent Imaging Innovations) using a 63× 1.4 NA objective and projected as described for the VD neurons.

RESULTS

All motoneuron commissures have defects in *mig-15 C. elegans* mutants

We wondered whether cholinergic motoneurons of the DA, DB, VA and AS classes, which also send commissural processes towards the DNC, require MIG-15 activity in the same way as D-type neurons. Using motoneuron-specific GFP markers, we found commissural defects for each class of motoneuron in the *mig-15(rh148)* mutant (Fig. 1B-G). Defects comprised abnormal left-right localization, additional branches, aberrant trajectories or failure to connect to the DNC. The proportion of defective commissures was 41% in VD/DD neurons (n=70); 25% in DA and DB neurons (n=73); and 30% in VA and AS neurons (n=62). These observations indicate that all dorsally projecting commissural motor axons require *mig-15*.

mig-15 mutants have multiple classes of VD/DD GABAergic commissural defects

Commissural defects were classified in order to understand their potential mechanistic origin, using the well-described D-type motoneurons as a model system for this study (Knobel et al., 1999). We fluorescently labeled the body wall muscles (BWM) and the lateral nerve fascicles (LNF), and examined the VD/DD commissural trajectory relative to these obstacles (Fig. 2A-F). In wild-type animals, commissures maintained a dorsal-ventral path upon crossing BWMs (Fig. 2B) and the LNF (Fig. 2C). In *mig-15(rh148)* mutants, however, many commissures either arrested (Fig. 2D,E) or extended along the LNFs (Fig. 2F). The position at which commissures arrested or changed orientation coincided with BWM boundaries (50%; Fig. 2G) and the LNF (75%; Fig. 2H). The total percentage of defects is greater than 100% because many LNFs are located at muscle edges (Fig. 2A). As there was 20% more fasciculation at the dorsal sub-lateral LNF than at the dorsal BWM, the commissural axons might mainly fasciculate with longitudinal axon bundles. In addition, 25% of defects were not colocalized with nerve fascicles (Fig. 2H). This might reflect commissure interactions with epidermal cells or new obstacles arising in the *mig-15* mutant background. Overall, our observations suggest that longitudinal obstacles affect the progression of *mig-15* VD/DD growth cones.

We grouped together commissures that longitudinally fasciculate and that prematurely arrest (class I). Additional classes include commissures with extra branches (class II) and commissures deviating from the normal dorsal-ventral orientation by >45° (class III). The three classes of defects are depicted in Fig. 2I.

We then compared the commissural defects in the three described *mig-15* mutants (Shakir et al., 2006). In the hypomorphic *mig-15(rh148)* mutant, 97% of the commissures reached the dorsal nerve cord (DNC), and <10% displayed class I-III defects (Fig. 2J). The strong *mig-15(rh80)* and null *mig-15(rh326)* mutants had moderate defects: class I and II defects occurred twice as often (Fig. 2J). These data confirmed that loss of *mig-15* function induces various commissural defects, and indicate that, even in strong mutants, most axons can reach the DNC. As strong *mig-15* mutants are difficult to maintain and have only slightly more defects than the *rh148* mutant, we used the latter to investigate further the origin of VD/DD commissural defects.

Class I and II VD axon defects are developmental

The pleiotropic axonal phenotype described above in *mig-15* L4 larvae could be explained by two non-mutually exclusive mechanisms. Axonal defects might be developmental and result from impaired neurite outgrowth, or they might result from a post-developmental defect such as defective maintenance or axonal regeneration, as was described for *unc-119* or *unc-70* mutants (Knobel et al., 2001; Hammarlund et al., 2007).

To address this issue, we compared commissural defects immediately after commissure outgrowth (late L2 larvae) and in L4 larvae (Fig. 3A). Class I and II defects were equally frequent in early

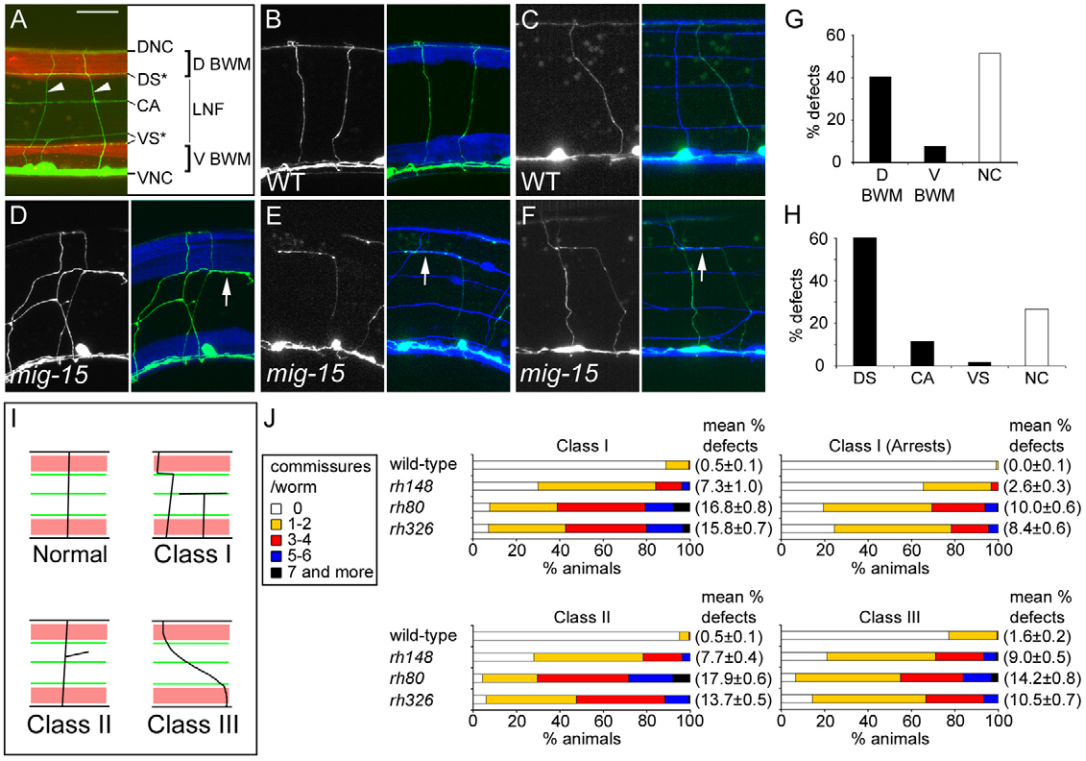

Fig. 2. Classes of defects in the commissures of *mig-15 C. elegans* mutants. (**A**) Longitudinal landmarks in a wild-type L4 larva. Dorsal side is up, anterior is to the right. In green, DNC, VNC, dorsal sublateral LNF (DS), canal-associated LNF (CA) and ventral sublateral LNF (VS). In red, dorsal (D) and ventral (V) BWM. Arrowheads indicate commissures; asterisks indicate the LNF colocalized with muscle edges. Dim punctae seen around commissures are autofluorescent gut granules. (**B-F**) Normal (B,C) and defective (D-F) VD/DD commissural trajectories (green) relative to body wall muscles (blue in right panels of B,D) and to longitudinal nerve fascicles and other commissures (blue in right panels of C,E,F) in wild-type (WT; B,C) and *mig-15(rh148)* (D-F) larvae. Arrows indicate a commissure fasciculated at the dorsal BWM (D), at the DS LNF (E) and transiently fasciculated with the DS LNF, but reaching the DNC (F). Scale bar: 25 μm. (**G**,**H**) Proportions of commissures with anterior-posterior fasciculation at the BWM boundaries (G, *n*=21 animals), at the level of LNF (H, *n*=60 animals) or at a non-colocalized position (NC; G,H) in *mig-15(rh148)* mutants. (**I**) Schematic of the three classes of commissural defects. See text for description. Red, BWM; green, LNF. (**J**) Penetrance of the VD/DD commissural defects per animal for each class in *mig-15* mutants. Numbers in parentheses on the right of each bar are the mean percentage of defective commissures per worm ± s.e.m. (100% is 19 defective VD/DD commissures). *n*>180 worms for each strain.

L2 and in L4 animals, indicating that they appeared during neurite outgrowth. By contrast, the frequency of class III defects increased with time, indicating that they mainly result from a progressive alteration of commissure trajectories. Presumably, *mig-15* mutant larvae accumulate other morphogenetic defects as they grow.

Cell-specific RNAi experiments suggest that *mig-15* requirement is cell-autonomous in VD/DD motoneurons (Poinat et al., 2002). To unambiguously establish cell autonomy, we rescued *mig-15* defects by driving MIG-15 expression in VD/DD neurons using the D-type specific *unc-25* promoter (Jin et al., 1999). The *Punc-25::mig-15* transgene led to dose-dependent class I defects in wild-type animals, suggesting that MIG-15 overexpression can be toxic. In *mig-15(rh148)* mutants, the transgene rescued the developmental class I and II defects, but not class III defects (Fig. 3B). These data confirm that class I and II defects result from a cell-autonomous loss of *mig-15* function and suggest that class III defects result from impaired *mig-15* functions in other tissues.

Abnormal growth cone migration leads to class I and II VD commissural defects

To confirm that class I and II defects are linked to abnormal axonal migration, we performed time-lapse imaging of growing VD neurites in *mig-15(rh148)* mutants as well as in animals overexpressing MIG-15. VD growth cones normally migrate rapidly below the epidermis and stall at the level of longitudinal obstacles in wild-type animals (Knobel et al., 1999) (Fig. 4A; see Movie 1 in the supplementary material). In *mig-15* mutants, VD growth cones migrated from the VNC to the DNC in a directional fashion, confirming that the majority of class III defects do not result from impaired ventral-dorsal guidance. However, they displayed an abnormal morphology and decreased motility (Fig. 4B,C; see Movies 2-4 in the supplementary material). Indeed, 25% of the *mig-15(rh148)* growth cones had extra branches with protrusive activity at their tips, many of which failed to retract (*n*=15 cones; see Movies 2, 3 in the supplementary material). In addition, *mig-15* growth cones abnormally spread at the level of dorsal sub-lateral obstacles and maintained a protrusive activity at their anterior or posterior tips leading to anterior-posterior elongation (see Movie 4 in the supplementary material). Failure to retract extra branches is likely to result in class II defects, whereas longitudinal outgrowth could lead to class I defects. Interestingly, loss of function and overexpression of MIG-15 led to similar phenotypes, suggesting that the level of MIG-15 and/or its polarized activity is needed for proper migration (Fig. 4D; see Movies 5, 6 in the supplementary material). Abnormal protrusive activity might perturb growth cone reorganization and lead to

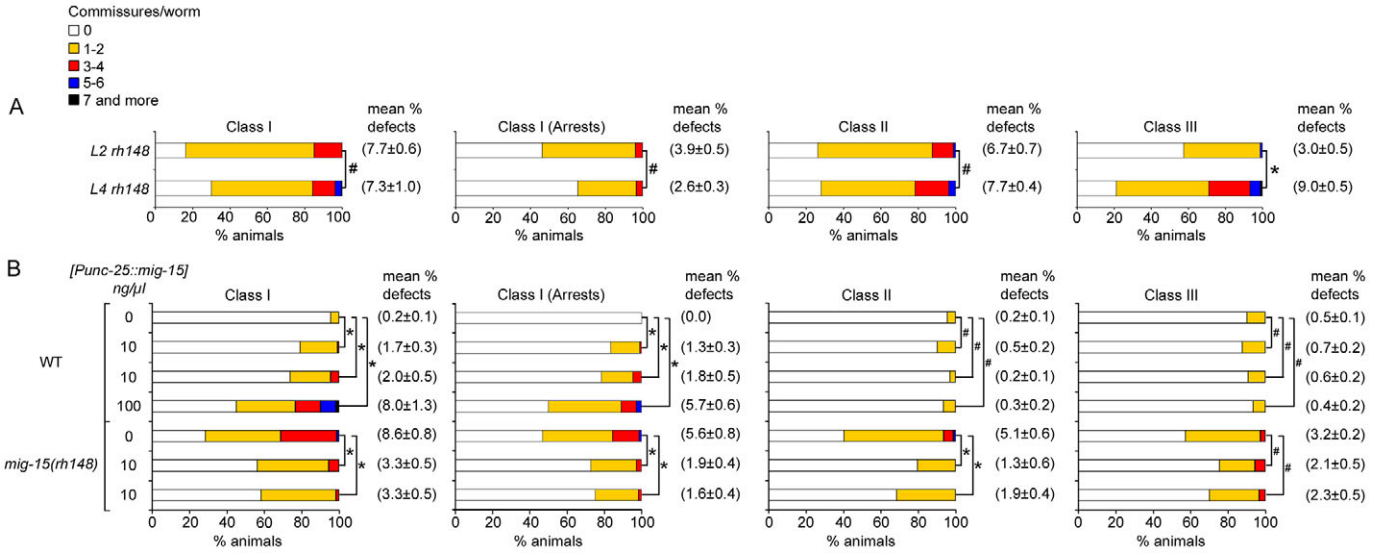

Fig. 3. VD commissural defects are developmental. (**A**) Penetrance of VD/DD commissural defects for each class in early L2 (end of VD commissures outgrowth) and L4 *mig-15(rh148) C. elegans* larvae. (**B**) A *[Punc-25::mig-15]* construct induced a dose-dependent phenotype in the wild-type background, and cell-autonomously rescued *mig-15(rh148)* VD/DD commissural defects. Concentrations of *Punc-25::mig-15* vector injected are indicated in ng/µl. Results are shown for two independent transgenic lines. *n*>80 worms for each strain. Numbers in parentheses on the right of each bar are the mean percentage of defective commissures per worm ± s.e.m. **P*<0.005; #, not significantly different; determined by *t*-test.

obstacle-crossing defects and abnormal fasciculation with the LNF. This interpretation predicts that arrested class I commissures reflect severe defects in growth cone polarized protrusive activity.

A genetic screen for *mig-15* enhancers identifies cytoskeleton regulators

Despite their structural growth cone defects, most VD commissures could reach the DNC in *mig-15* null mutants (Fig. 2J), suggesting that compensatory or redundant mechanisms ensure proper outgrowth. To identify genes acting in the same pathway or in parallel to *mig-15*, we performed an RNAi-based *mig-15(rh148)* enhancer screen (see Table S1 in the supplementary material). Genes acting in parallel are expected to be strong *mig-15* enhancers, whereas genes acting in the same pathway should behave as weak enhancers that increase the penetrance of *mig-15(rh148)* commissural defects to that of *mig-15* null mutants.

The downregulation of many candidate genes known to control axonal migration induced commissural defects independently of *mig-15*, thus confirming the RNAi efficiency in D-type motoneurons (see Table S2 in the supplementary material). Interestingly, we identified eight *mig-15* enhancers among genes that had not been previously implicated in *C. elegans* neuronal development, although their closest vertebrate homologs have often been shown to regulate growth cone migration. These genes encode the actin regulators ERM-1 (the only *C. elegans* ezrin/radixin/moesin homolog) and WVE-1 (the ortholog of WAVE/SCAR/WASF1), the microtubule-binding proteins BICD-1 (a Bicaudal D homolog), the motor protein UNC-116 (the kinesin-1 heavy chain/KIF5 ortholog) and its partner UNC-33 (collapsin response mediator protein 2/DPYSL2 ortholog), the MAPK cascade scaffolding protein UNC-16 (JSAP1/JIP3/MAPK8IP3 homolog), KGB-1 (a JNK MAPK homolog) and LET-502 (Rho-binding kinase homolog).

Homologs of some of the identified enhancers are known partners of MAP4K4 in other systems. Kinesin-1 and WAVE form a complex in vertebrates, which regulates neuronal actin dynamics and axon outgrowth (Kawano et al., 2005). In *C. elegans*, WVE-1, UNC-116 and the kinesin-1 partner UNC-33/CRMP-2 are also required for axon outgrowth (Li et al., 1992; Withee et al., 2004; Schmitz et al., 2007). Bicaudal D genetically interacts with Msn in *Drosophila* (Houalla et al., 2005), and the JNK MAPK pathway is activated by MAP4K4 kinases in yeast, *Drosophila* and mammals (Dan et al., 2001). We failed to confirm the genetic interactions between *mig-15* and JNK MAPK or *bicd-1* using mutations (see Fig. S1 in the supplementary material). We favor the hypothesis that JNK MAPK signaling is not involved downstream of MIG-15 during growth cone migration, because the confirmed *mig-15* enhancer *unc-16* (see Fig. S2A-D in the supplementary material) is likely to act non-autonomously (see Fig. S2E in the supplementary material).

The UNC-116–WVE-1 complex acts in parallel to *mig-15*

We investigated the involvement of the strong *mig-15* enhancers *unc-116*, *unc-33* and *wve-1* in D-type motoneuron commissural outgrowth. On their own, the hypomorphic *unc-116(e2310)* and *unc-33(e204)* mutants displayed 3-6% arrested class I commissures (Fig. 5A). Consistent with RNAi results, double mutants combining *unc-116* or *unc-33* mutations with *mig-15(rh148)* displayed strong synthetic axon outgrowth defects, which were more penetrant than in the *mig-15* null allele. We thus suggest that MIG-15 does not act by regulating the kinesin-1 complex, but that it acts in parallel to UNC-116 and UNC-33. We could not test the extent of enhancement in the *mig-15* null mutant, because it displayed 100% embryonic lethality with *unc-116* or *unc-33* mutations (Fig. 5A).

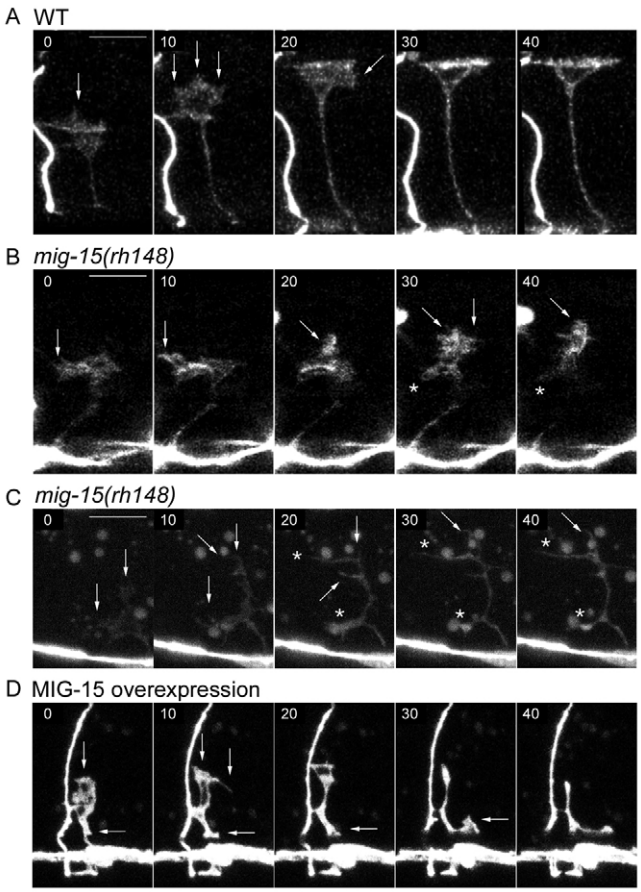

Fig. 4. Abnormal growth cone protrusive activity in *mig-15* mutants. Time-lapse confocal imaging of VD growth cone migration in wild-type (WT; **A**), in *mig-15(rh148)* (**B**,**C**) and in *[Punc-25::mig-15]* transgenic L2 larvae (MIG-15 overexpression; **D**). Time is indicated in minutes on each frame. Arrows indicate zones of protrusive activity. In the *mig-15* mutants, protrusive activity was also observed along unretracted extra branches (asterisks). Scale bars: 5 μm.

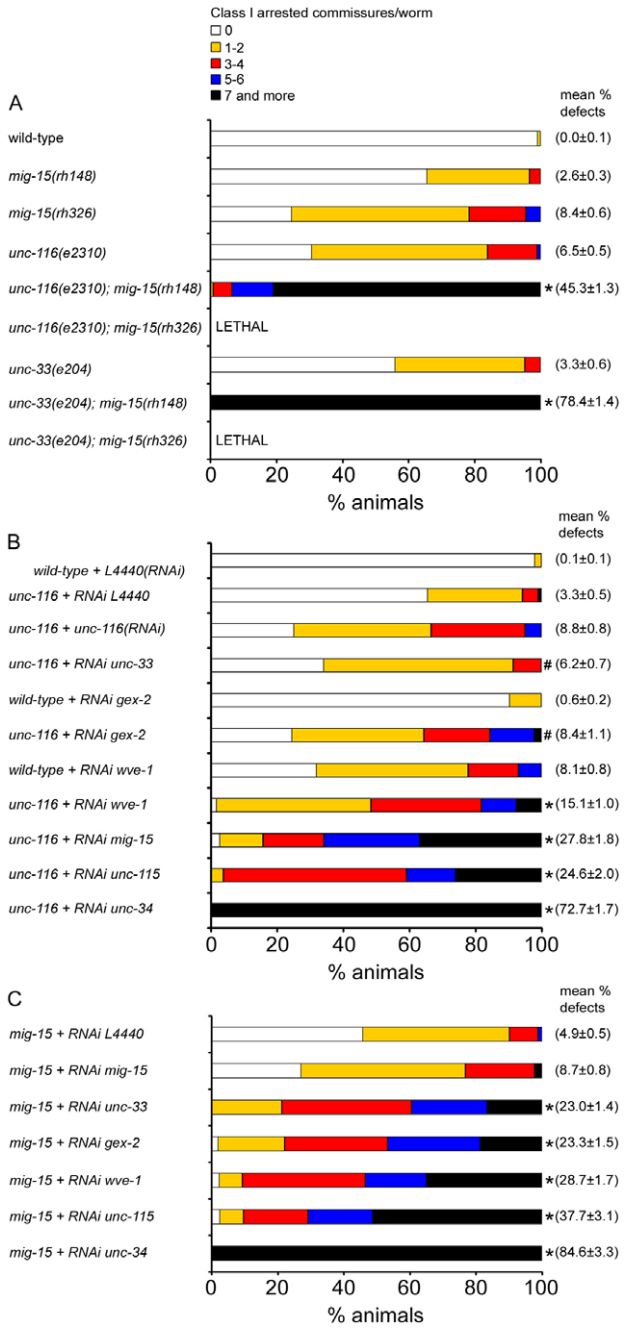

Fig. 5. Kinesin-1-WAVE complex genes act in parallel to *mig-15*. Scoring of class I arrested VD/DD commissures in: (**A**) *mig-15*, *unc-116* and *unc-33* mutants; (**B**) UNC-116–WVE-1 complex RNAi in wild-type and *unc-116* backgrounds; and (**C**) UNC-116–WVE-1 complex RNAi in *mig-15* background. (B,C) RNAi against *unc-34* and *unc-115* (encoding ENA/VASP and AbLIM orthologs, respectively) synthetically enhanced both *mig-15* and *unc-116* mutants, indicating that *unc-34* and *unc-115* act in parallel to both genes. *unc-115(RNAi)* and *unc-34(RNAi)* were used as positive controls. A bacterial clone carrying the empty vector L4440 was used as negative control. Results were gathered from at least three independent experiments for each RNAi clone. Numbers in parentheses on the right of each bar indicate mean percentage of defective commissures per worm ± s.e.m. $n>100$ worms for each mutant strain and RNAi experiment. *$P<0.001$ determined by *t*-test, significant enhancement compared with (A) *mig-15(rh326);* (B) *mig-15+mig-15(RNAi)*; (C) *unc-116+unc-116(RNAi)* phenotypes. #$P>0.1$ determined by *t*-test, no significant difference between *unc-116 RNAi* and *unc-116* mutant phenotypes in C.

To bypass embryonic lethality and confirm that MIG-15 and the UNC-116–WVE-1 complex act in parallel, we performed reciprocal RNAi experiments in *unc-116(e2310)* and *mig-15(rh148)* mutants (Fig. 5B-C). As expected, *mig-15(RNAi)* synthetically enhanced the *unc-116* phenotype. RNAi against *unc-33*, *unc-116*, *gex-2* (encoding the homolog of the WAVE complex component Sra1, GEX-2) and *wve-1* synthetically enhanced the *mig-15(rh148)* defects, confirming that all these genes act in parallel to *mig-15* (Fig. 5C). RNAi against *unc-33* and *gex-2* in the *unc-116* mutant did not lead to a significant increase in arrested commissure frequency compared with *unc-116* and *unc-116(RNAi)*, which is in agreement with a model in which UNC-116, GEX-2 and UNC-33 form a complex (Fig. 5B). *wve-1(RNAi)* significantly aggravated the *unc-116* mutant commissural phenotype, contrary to expectations, perhaps because it is more efficient than *gex-2(RNAi)*, to eliminate the entire UNC-116–WVE-1 complex in the *unc-116(e2310)* background (Fig. 5B). Altogether, these data strongly suggest that the UNC-116–WVE-1 complex and MIG-15 act in parallel during VD/DD neurite outgrowth.

Loss of ERM-1 function enhances *mig-15* defects

erm-1 was a weak *mig-15* enhancer identified in our screen (see Table S2 in the supplementary material). In *C. elegans*, *erm-1* mutants have junction remodeling defects and loss of apical actin

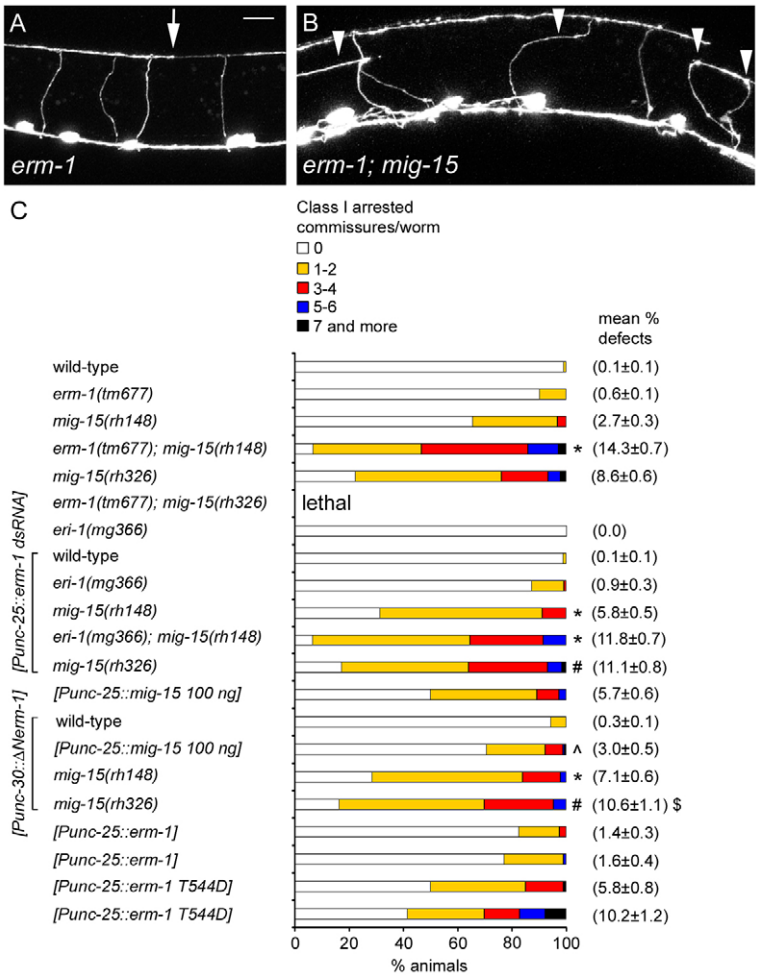

Fig. 6. The moesin ortholog *erm-1* is a cell-autonomous *mig-15* enhancer acting in the same genetic pathway. (**A**,**B**) VD/DD commissural phenotype in *erm-1(tm677)* mutant (A) and *erm-1(tm677); mig-15(rh148)* double mutant (B) larvae. Arrow in A indicates underextension defect in the DNC. Arrowheads in B indicate class I defective commissures. Scale bar: 25 μm. (**C**) Quantification of class I arrested commissural defects in *erm-1* and *mig-15* mutants, and in animals carrying transgenes inducing VD/DD-specific *erm-1(RNAi)*, expression of ΔN-ERM-1::GFP and of a constitutively activated ERM-1(T544D). Numbers in parentheses on the right of each bar indicate mean percentage of defective commissures per worm ± s.e.m. *n*>100 worms for each strain, except $, *n*=65. **P*<0.001 determined by *t*-test, significant enhancement of the *mig-15(rh148)*; ^*P*<0.001 determined by *t*-test, suppression of the *[Punc-25::mig-15]* (^) phenotypes; #, not significantly different from *mig-15(rh326)*.

in epithelia, leading to early larval lethality (Göbel et al., 2004; Van Fürden et al., 2004). However, this phenotype is maternally rescued and neuronal defect analysis is possible in *erm-1* homozygous mutants born from heterozygous mothers. ERM proteins are involved in axonal migration in vertebrates (Ramesh, 2004) and ERM-1 was recently shown to regulate axon outgrowth in one *C. elegans* neuron (Norris et al., 2009). *erm-1(tm677)* single mutants had only subtle VD/DD commissural defects, such as D-type commissure under-extension in the DNC (Fig. 6A). Despite this mild phenotype, the *erm-1* mutation doubled the penetrance of class I and II defects in *mig-15(rh148)*, leading to 15% arrested commissures (Fig. 6B,C), which is the penetrance observed in *mig-15* strong and null phenotypes (Fig. 2J). In addition, we observed that 30% *erm-1(tm677);mig-15(rh148)* embryos died with morphology defects suggesting that these genes might also act in parallel during embryogenesis (J.T., unpublished).

erm-1 functions cell-autonomously in the same pathway as *mig-15*

As *erm-1* is a weak *mig-15* enhancer, both genes might act in the same pathway during VD/DD neurite outgrowth. To test this hypothesis, we used several parallel strategies. First, as an alternative to a combination of the null alleles *erm-1(tm677)* and *mig-15(rh326)*, which produced dead embryos (Fig. 6C), we specifically induced RNAi in D-type neurons by driving *erm-1* dsRNA under the *unc-25* promoter. D-type-specific *erm-1(RNAi)* did not significantly aggravate the phenotype of the strong *mig-15* alleles *rh326* and *rh80*, but significantly enhanced that of the weak allele *mig-15(rh148)* (Fig. 6C), suggesting that *erm-1* acts cell-autonomously in the same pathway as *mig-15*. This enhancement was even greater in the RNAi-hypersensitive *eri-1* mutant background, indicating that the transgene effect is RNAi-dependent.

Second, because vertebrate NIK appears to activate ezrin by phosphorylating it at position T567 (Baumgartner et al., 2006), we tried to define whether ERM-1 could represent a MIG-15 target. We found, unfortunately, that *Punc-25::erm-1* constructs killed *erm-1(tm677)/+; mig-15(rh148)* animals, and that the expression of a constitutively active ERM-1(T544D) form (equivalent to EzrinT567D) induced premature commissure arrest. As an alternative approach, we reasoned that overexpression of a truncated ERM-1 containing only the C-terminal region with the potential T544 phosphorylation site (ΔN-ERM-1) might antagonize the effect of MIG-15 overexpression by providing more substrate to titrate out MIG-15 kinase activity. A transgene driving ΔN-ERM-1::GFP expression under the GABAergic motoneuron specific *unc-30* promoter (Jin et al., 1994) was indeed able to partially suppress the MIG-15 overexpression phenotype (Fig. 6C). Furthermore, the *Punc-30::ΔN-ERM-1::GFP* transgene induced class I arrests at low penetrance in wild-type animals, probably by interfering with endogenous MIG-15 activity, and aggravated the commissural defects of the hypomorph *mig-15(rh148)*, but not of the null *mig15(rh326)* mutants. Taken together, these results suggest that ERM-1 is a MIG-15 substrate.

mig-15 and *unc-5* might act in the same pathway

Finally, we wanted to determine whether *mig-15* acts in the same process as the netrin receptor UNC-5. In *unc-5(e53)* null mutants, almost all commissures failed to reach the DNC, whereas in *unc-5(e152)* mutants, many commissures reached the DNC in ~90% of the animals (see Fig. S3 in the supplementary material). *mig-15(rh148)* enhanced the phenotype of *unc-5(e152)*, but not that of *unc-5(e53)* (see Fig. S3 in the supplementary material). We conclude that *mig-15* and *unc-5* are likely to act in the same genetic pathway during dorsalward growth cone migration.

The protrusive activity of VD growth cones is abnormal in *mig-15*, *unc-116* and *erm-1* mutants

To confirm that *mig-15* and its enhancers regulate VD growth cone protrusive activity, we extended our time-lapse analysis to include the *unc-116* and *erm-1* mutants. We observed abnormal growth cone migration in both mutants, suggesting that both genes are required at the time of axonal outgrowth. The *erm-1* growth cones displayed defective migration despite persistent protrusive activity (Fig. 7A; see Movie 7 in the supplementary material) or more subtle defects, such as transient loss of the growth cone structure (see Movies 8 and 9 in the supplementary material). In *unc-116* mutants, growth cones migrated slowly with reduced protrusive activity and sometimes collapsed before reaching the dorsal BWM (Fig. 7B; see Movies 10-12 in the supplementary material). Unlike *mig-15* mutants, none of these mutants displayed unretracted extra branches.

Stable protrusions at the leading edge are required for directional cell migration (Petrie et al., 2009). Therefore, the protrusive activity was quantified in the proximal and distal halves of wild-type and mutant growth cones (see Movie 11 in the supplementary material; Fig. 7C). In wild-type growth cones, we measured roughly six times more protrusions per minute in the distal half of the growth cone than in the proximal half (Fig. 7C). *mig-15* mutants displayed overall more protrusive activity in the proximal half, and, consistent with the grouping of *mig-15* and *erm-1* in the same pathway, *erm-1* mutants showed a similar phenotype. By contrast, *unc-116* mutants had reproducibly fewer membrane protrusions in the distal growth cone but a normal rate of protrusive activity in the proximal part (Fig. 7C). On average, growth cone protrusive activity was less polarized toward the leading edge in all three mutants analyzed, as indicated by the distal to proximal ratio of protrusive activities (Fig. 7C). Altogether, these data suggest that UNC-116 is required to stimulate protrusive activity at the leading edge. In addition, these results indicate that MIG-15 and ERM-1 are necessary to maintain a low protrusive activity at the rear of the growth cone.

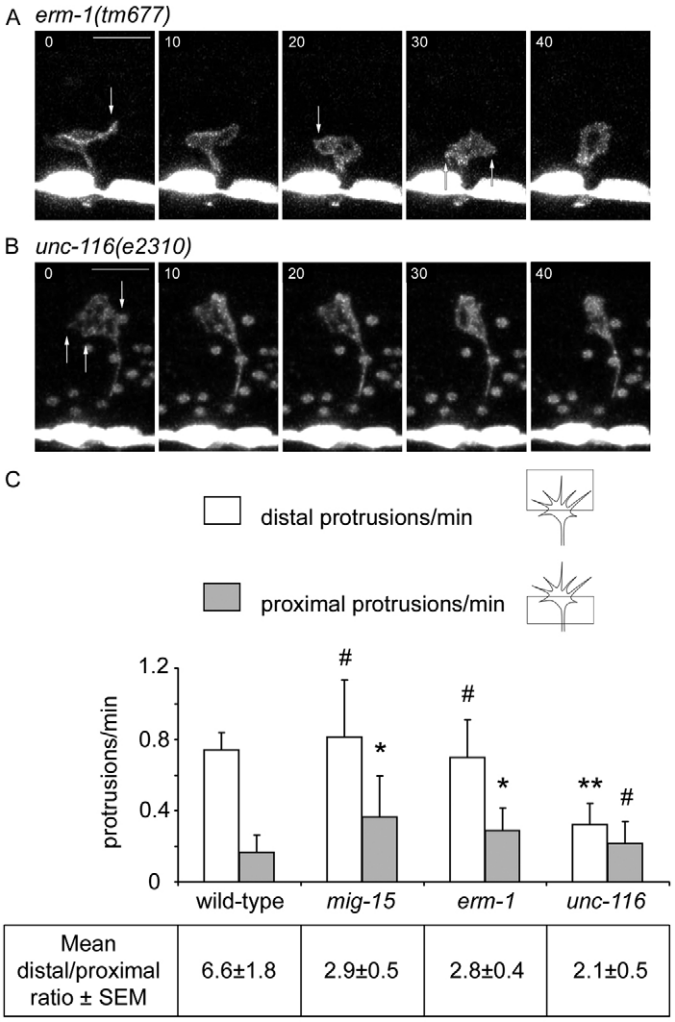

Mean distal/proximal ratio ± SEM	6.6±1.8	2.9±0.5	2.8±0.4	2.1±0.5

Fig. 7. Abnormal protrusive activity in VD growth cones of *mig-15*, *unc-116* and *erm-1* mutants. (**A**,**B**) Time-lapse confocal imaging of VD growth cone migration in *erm-1(tm677)* (A) and in *unc-116(e2310)* (B) larvae. Time is in minutes on each frame. Arrows indicate zones of protrusive activity. Scale bars: 5 μm. (**C**) Mean number of VD growth cones protrusions per minute in the distal and proximal halves of growth cones and mean ratio of protrusive activity between the distal and the proximal halves of VD growth cones. Error bars indicate s.e.m. Number of growth cones scored: wild type, 9; *mig-15*, 8; *erm-1*, 9; *unc-116*, 13. **P*<0.05; ***P*<0.001, determined by *t*-test, significant difference compared with the wild-type phenotype. #, not significantly different.

mig-15 regulates HSN polarity during ventral migration

If, as suggested above, MIG-15 contributes to polarize the growth cone, its activity should influence the polarized distribution of some growth cone markers. To test this idea, we turned our attention to the lamellipodin homolog MIG-10, which is polarized at the leading edge during the outgrowth of some axons (Adler et al., 2006; Quinn et al., 2006). In our hands, expression of MIG-10::YFP under the D-type promoter *unc-25* induced axon defects. We therefore relied on the hermaphrodite specific neuron (HSN), in which MIG-10::YFP localization was originally characterized. First, we investigated whether *mig-15* is required for the ventrally directed outgrowth of the HSN axon. We found that all HSN axons in *mig-15(rh148)* mutants could reach the VNC, but displayed at low penetrance structural defects analogous to class I and II commissural defects (see Fig. S4A,B in the supplementary material). Rescue experiments suggest that *mig-15* functions cell-autonomously in the HSN, as in D-type neurons (see Fig. S4B in the supplementary material). Similar defects were observed for the ventrally directed axons of the touch neurons AVM and PVM (class I defects: 5% in AVMs, 8% in PVMs; class II defects: 5% in AVMs and PVMs; n=101 for AVMs, n=98 for PVMs). Thus, MIG-15 is also important for ventral axon outgrowth. In HSN neurons, whereas MIG-10::YFP always showed a polarized localization in control L3 larvae, its localization was perturbed in *mig-15* L3 larvae, with persistent patches of MIG-10::YFP on the dorsal side of the growth cone (see Fig. S4C,D in the supplementary material).

These results suggest that MIG-15 maintains the growth cone protrusive polarity of both ventrally migrating neurons and dorsally migrating commissural axons.

DISCUSSION

Using genetics and time-lapse microscopy, we have shown that MIG-15 is required cell-autonomously for neurite outgrowth in *C. elegans*. Our analysis suggests that *mig-15* commissural defects primarily result from a polarity defect within the growth cone affecting its motility and its ability to cross longitudinal obstacles. Our genetic results identified genes acting presumably in the same pathway as *mig-15* and others acting in parallel. Contrary to what was found in other systems (Dan et al., 2001; Machida et al., 2004), our data suggest that MIG-15 does not control a JNK pathway during commissure outgrowth. Although we identified the JNK adaptor UNC-16 as a *mig-15* enhancer, we could not demonstrate any obvious implication of JNK kinases during VD growth cone migration. Instead, our data suggest that *unc-16* acts non-cell autonomously (see Fig. S2 in the supplementary material). The rare commissural class II defects observed in JNK pathway mutants might be associated with defects in stress resistance, a well-documented JNK function in *C. elegans* (Kim et al., 2004; Mizuno et al., 2004).

MIG-15 acts in parallel to the WAVE actin regulator WVE-1 to allow robustness of directional migration

We observed severe perturbation of growth cone morphology in *mig-15* mutants and, paradoxically, relatively mild defects in the final commissures, which indicates that compensatory mechanisms can repair those defects and ensure the robustness of axonal outgrowth. Intriguingly, like *mig-15* mutants, *unc-116* mutants have impaired growth cone motility but very few commissural defects. We showed that UNC-116 and UNC-33 act in parallel to MIG-15 and that UNC-116 maintains active protrusions at the leading edge of the VD growth cone. Consistently, WAVE has been shown to localize at the leading edge of the growth cone in mouse cerebellar granule neurons (Tahirovic et al., 2010). Kinesin-1 and CRMP-2 are involved in the transport of the actin regulator Sra1-WAVE complex from the neuron cell body to the growth cone (Arimura and Kaibuchi, 2007). The kinesin-1-WAVE complex can regulate neurite outgrowth in mammalian neurons (Kawano et al., 2005) and our study reveals the evolutionary conservation of this function. Altogether, our results suggest a conserved role for the MIG-15 kinase and the UNC116/WVE-1 pathway in promoting directional growth cone migration by locally regulating actin dynamics at opposite sites of the growth cone (Fig. 8). The complementary activities of MIG-15 and UNC-116 pathways might allow for functional compensation, resulting in mostly normal axon morphology when only one of the pathways is compromised.

MIG-15 and ERM-1 prevent membrane protrusions at the rear of the growth cone

erm-1 was identified as a weak *mig-15* enhancer and our genetic analysis suggests that *mig-15* and *erm-1* act in the same genetic pathway during VD growth cone migration. In addition, both *erm-1* and *mig-15* mutants displayed abnormal protrusive activity at the rear of the growth cone. It is tempting to speculate that MIG-15 could directly activate ERM-1 at the rear of the migrating growth cone, because, as mentioned above, mammalian NIK can activate ERM proteins by phosphorylating a threonine residue (Baumgartner et al., 2006) that is also present in ERM-1. In support of this notion, overexpression of MIG-15 and constitutive activation of ERM-1 both led to class I arrested commissural defects, which we showed to be a hallmark of defective protrusive polarity in the growth cone. Moreover, cell-specific overexpression of the ERM-1 C-terminal domain (containing the conserved threonine residue) can suppress the MIG-15 overexpression phenotype. We thus propose that MIG-15 phosphorylates and activates ERM-1, which can eventually crosslink actin and plasma membrane. We hypothesize that ERM-1 activation is coupled to inhibition of actin dynamics at the rear of the growth cone. Our results suggest that the regulation of ERM proteins and actin dynamics by MAP4K4 could be a conserved mechanism contributing to directed cell migration. The lack of extra branches in the commissures of *erm-1* mutants suggests that MIG-15 regulates branch retraction independently of ERM-1.

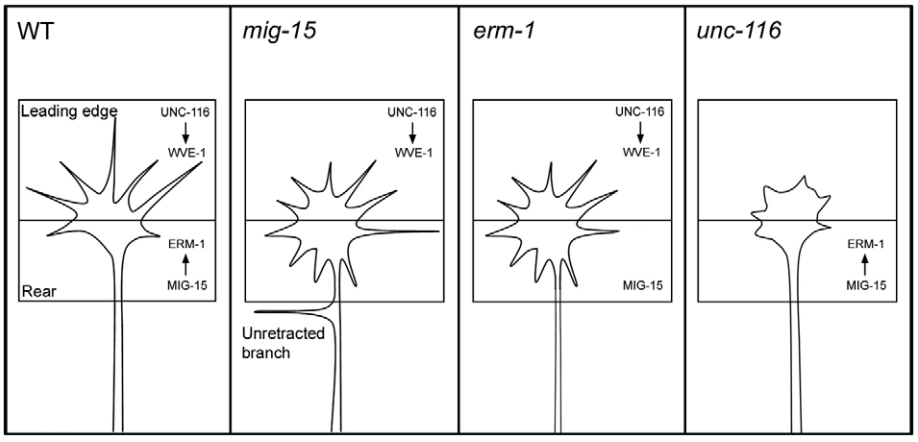

Fig. 8. Model in which UNC-116–WVE-1 and MIG-15–ERM-1 complementarily regulate growth cone polarity. We propose a model in which MIG-15 activates ERM-1 to suppress protrusions at the rear of VD growth cones whereas the UNC-116–WVE-1 complex stimulates actin dynamics at the leading edge. These two parallel pathways establish a distal to proximal polarity of actin-driven protrusive activity. Impairment of any pathway would lead to depolarized protrusive activity, reduced growth cone migration speed and failure to cross longitudinal obstacle boundaries, leading to premature longitudinal fasciculation. In addition, the *mig-15* mutants growth cones fail to retract extra branches. Extra-branch retraction seems to be independent of ERM-1 function.

MIG-15 is required broadly to set up polarized migration in response to guidance cues

We and others (Shakir et al., 2006) observed the same classes of outgrowth defects in the motoneuron commissures, HSN, AVM, PVM and PDE axons of *mig-15* mutants. Thus, MIG-15 should have a general function in polarizing growth cones. Axonal outgrowth along the dorsal-ventral axis is guided by the activity of UNC-6 through the UNC-5 and UNC-40 receptors. Although the molecular mechanisms mediating UNC-5 signal transduction are not fully understood, those acting downstream of UNC-40 in ventral-directed outgrowth have been well characterized (Gitai et al., 2003; Adler et al., 2006; Chang et al., 2006; Quinn et al., 2006; Quinn et al., 2008). One specific outcome of UNC-40 signaling is Rac GTPase activation and MIG-10 recruitment at the leading edge of the growth cone in response to the attractive netrin cue (Adler et al., 2006; Quinn et al., 2006; Quinn et al., 2008). We found that MIG-15 is required for polarized MIG-10 localization, indicating that MIG-15 could function downstream of UNC-6 and UNC-40 in ventral guidance. Because our data suggest that *mig-15* acts in the *unc-5* pathway (see Fig. S3 in the supplementary material), we propose that MIG-15 also contributes to polarization of the growth cone away from the UNC-6 repellent in dorsal-directed axon outgrowth.

How does MIG-15 contribute to the establishment of polarity? Because MIG-15 regulates Q neuroblast polarity (Chapman et al., 2008), a process that requires UNC-40 but not UNC-6 (Honigberg and Kenyon, 2000), one possibility is that MIG-15 regulates the activity or amount of the UNC-40 receptor, which we found to induce commissural class I arrest when overexpressed (J.T., unpublished). As *mig-15* and *erm-1* were identified in genetic screens for endocytosis regulators (Balklava et al., 2007), MIG-15 might regulate UNC-40 localization through its endocytosis at the rear of the growth cone to ensure that dorsal-directed growth cones only respond to UNC-5.

A second possibility is that Rho and Rac GTPases are generally considered to have antagonistic activities in the growth cone (Hall and Lalli, 2010). Thus, *mig-15* and *erm-1* might act in a Rho/ROCK pathway to prevent Rac activation and MIG 10 accumulation at the rear of the growth cone. Interestingly, inhibition of the ROCK homolog LET-502 weakly enhanced *mig-15* commissural defects in our enhancer screen, indicating that *let-502* and *mig-15* might act in the same genetic pathway (see Table S2 in the supplementary material).

A third possible mechanism involves integrin adhesion receptors, which have been shown to bind to MIG-15 (Poinat et al., 2002). Moreover, both *ina-1* (alpha-integrin) and *mig-15* mutants have strikingly similar commissural defects (Poinat et al., 2002) (J.T., unpublished). A recent study showed that myelin-associated glycoprotein chemorepulsive response of axonal growth cones is mediated by asymmetric endocytosis of integrin receptors on the repellent side (Hines et al., 2010). MIG-15 and ERM-1 might similarly control integrin endocytosis at the rear of the growth cone in response to UNC-6. Future experiments specifically designed to test these hypotheses will be necessary. In addition, unbiased approaches, such as *unc-116* or *erm-1* enhancer screens, are likely to identify new components of the MAP4K4 polarization machinery.

Acknowledgements

We thank Drs Jean-Louis Bessereau, Hanna Fares, Yishi Jin, Cornelia Bargmann, Olaf Bossinger and Karla Knobel for strains, protocols and reagents; and Abby Dernburg for sharing a spinning disc microscope. Some nematode strains used in this work were provided by the *Caenorhabditis* Genetics Center, which is funded by the NIH National Center for Research Resources (NCRR). We are grateful to Imane Azzouzi for technical help during the RNAi enhancer screen; David Rodriguez for helping with confocal imaging; the Labouesse, Georges-Labouesse and Jarriault laboratories for constructive discussions and critical reading of the manuscript; and the IGBMC Imaging Center.

Funding

This work was supported grants from the Association pour la Recherche sur le Cancer, Association Française contre les Myopathies and the Agence Nationale pour la Recherche to M.L. and E.G.-L., from NIH to G.G. and postdoctoral fellowships from the Association pour la Recherche contre le Cancer and the Ligue Nationale Contre le Cancer to J.T. Deposited in PMC for release after 12 months.

Competing interests statement

The authors declare no competing financial interests.

Supplementary material

Supplementary material for this article is available at http://dev.biologists.org/lookup/suppl/doi:10.1242/dev.061952/-/DC1

References

Adler, C. E., Fetter, R. D. and Bargmann, C. I. (2006). UNC-6/Netrin induces neuronal asymmetry and defines the site of axon formation. *Nat. Neurosci.* **9**, 511-518.

Arimura, N. and Kaibuchi, K. (2007). Neuronal polarity: from extracellular signals to intracellular mechanisms. *Nat. Rev. Neurosci.* **8**, 194-205.

Balklava, Z., Pant, S., Fares, H. and Grant, B. D. (2007). Genome-wide analysis identifies a general requirement for polarity proteins in endocytic traffic. *Nat. Cell Biol.* **9**, 1066-1073.

Baumgartner, M., Sillman, A. L., Blackwood, E. M., Srivastava, J., Madson, N., Schilling, J. W., Wright, J. H. and Barber, D. L. (2006). The Nck-interacting kinase phosphorylates ERM proteins for formation of lamellipodium by growth factors. *Proc. Natl. Acad. Sci. USA* **103**, 13391-13396.

Brenner, S. (1974). The genetics of *Caenorhabditis elegans*. *Genetics* **77**, 71-94.

Chan, S. S., Zheng, H., Su, M. W., Wilk, R., Killeen, M. T., Hedgecock, E. M. and Culotti, J. G. (1996). UNC-40, a *C. elegans* homolog of DCC (Deleted in Colorectal Cancer), is required in motile cells responding to UNC-6 netrin cues. *Cell* **87**, 187-195.

Chang, C., Adler, C. E., Krause, M., Clark, S. G., Gertler, F. B., Tessier-Lavigne, M. and Bargmann, C. I. (2006). MIG-10/lamellipodin and AGE-1/PI3K promote axon guidance and outgrowth in response to slit and netrin. *Curr. Biol.* **16**, 854-862.

Chapman, J. O., Li, H. and Lundquist, E. A. (2008). The MIG-15 NIK kinase acts cell-autonomously in neuroblast polarization and migration in *C. elegans*. *Dev. Biol.* **324**, 245-257.

Chilton, J. K. (2006). Molecular mechanisms of axon guidance. *Dev. Biol.* **292**, 13-24.

Dan, I., Watanabe, N. M. and Kusumi, A. (2001). The Ste20 group kinases as regulators of MAP kinase cascades. *Trends Cell Biol.* **11**, 220-230.

Fleming, T., Chien, S. C., Vanderzalm, P. J., Dell, M., Gavin, M. K., Forrester, W. C. and Garriga, G. (2010). The role of *C. elegans* Ena/VASP homolog UNC-34 in neuronal polarity and motility. *Dev. Biol.* **344**, 94-106.

Gitai, Z., Yu, T. W., Lundquist, E. A., Tessier-Lavigne, M. and Bargmann, C. I. (2003). The netrin receptor UNC-40/DCC stimulates axon attraction and outgrowth through enabled and, in parallel, Rac and UNC-115/AbLIM. *Neuron* **37**, 53-65.

Göbel, V., Barrett, P. L., Hall, D. H. and Fleming, J. T. (2004). Lumen morphogenesis in *C. elegans* requires the membrane-cytoskeleton linker *erm-1*. *Dev. Cell* **6**, 865-873.

Hall, A. and Lalli, G. (2010). Rho and Ras GTPases in axon growth, guidance, and branching. *Cold Spring Harb. Perspect. Biol.* **2**, a001818.

Hamelin, M., Zhou, Y., Su, M. W., Scott, I. M. and Culotti, J. G. (1993). Expression of the UNC-5 guidance receptor in the touch neurons of *C. elegans* steers their axons dorsally. *Nature* **364**, 327-330.

Hammarlund, M., Jorgensen, E. M. and Bastiani, M. J. (2007). Axons break in animals lacking beta-spectrin. *J. Cell Biol.* **176**, 269-275.

Hatten, M. E. (2002). New directions in neuronal migration. *Science* **297**, 1660-1663.

Hines, J. H., Abu-Rub, M. and Henley, J. R. (2010). Asymmetric endocytosis and remodeling of beta1-integrin adhesions during growth cone chemorepulsion by MAG. *Nat. Neurosci.* **13**, 829-837.

Honigberg, L. and Kenyon, C. (2000). Establishment of left/right asymmetry in neuroblast migration by UNC-40/DCC, UNC-73/Trio and DPY-19 proteins in *C. elegans*. *Development* **127**, 4655-4668.

Houalla, T., Hien Vuong, D., Ruan, W., Suter, B. and Rao, Y. (2005). The Ste20-like kinase misshapen functions together with Bicaudal-D and dynein in driving nuclear migration in the developing drosophila eye. *Mech. Dev.* **122**, 97-108.

Ishii, N., Wadsworth, W. G., Stern, B. D., Culotti, J. G. and Hedgecock, E. M. (1992). UNC-6, a laminin-related protein, guides cell and pioneer axon migrations in *C. elegans*. *Neuron* **9**, 873-881.
Jin, Y., Hoskins, R. and Horvitz, H. R. (1994). Control of type-D GABAergic neuron differentiation by *C. elegans* UNC-30 homeodomain protein. *Nature* **372**, 780-783.
Jin, Y., Jorgensen, E., Hartwieg, E. and Horvitz, H. R. (1999). The *Caenorhabditis elegans* gene *unc-25* encodes glutamic acid decarboxylase and is required for synaptic transmission but not synaptic development. *J. Neurosci.* **19**, 539-548.
Kamath, R. S., Fraser, A. G., Dong, Y., Poulin, G., Durbin, R., Gotta, M., Kanapin, A., Le Bot, N., Moreno, S., Sohrmann, M. et al. (2003). Systematic functional analysis of the *Caenorhabditis elegans* genome using RNAi. *Nature* **421**, 231-237.
Kawano, Y., Yoshimura, T., Tsuboi, D., Kawabata, S., Kaneko-Kawano, T., Shirataki, H., Takenawa, T., Kaibuchi, K. (2005). CRMP-2 is involved in kinesin-1-dependent transport of the Sra-1/WAVE1 complex and axon formation. *Mol. Cell. Biol.* **25**, 9920-9935.
Keleman, K. and Dickson, B. J. (2001). Short- and long-range repulsion by the *Drosophila* Unc5 netrin receptor. *Neuron* **32**, 605-617.
Kennedy, S., Wang, D. and Ruvkun, G. (2004). A conserved siRNA-degrading RNase negatively regulates RNA interference in *C. elegans*. *Nature* **427**, 645-649.
Kim, D. H., Liberati, N. T., Mizuno, T., Inoue, H., Hisamoto, N., Matsumoto, K. and Ausubel, F. M. (2004). Integration of *Caenorhabditis elegans* MAPK pathways mediating immunity and stress resistance by MEK-1 MAPK kinase and VHP-1 MAPK phosphatase. *Proc. Natl. Acad. Sci. USA* **101**, 10990-10994.
Knobel, K. M., Jorgensen, E. M. and Bastiani, M. J. (1999). Growth cones stall and collapse during axon outgrowth in *Caenorhabditis elegans*. *Development* **126**, 4489-4498.
Knobel, K. M., Davis, W. S., Jorgensen, E. M. and Bastiani, M. J. (2001). UNC-119 suppresses axon branching in *C. elegans*. *Development* **128**, 4079-4092.
Köppen, M., Fernández, B. G., Carvalho, L., Jacinto, A. and Heisenberg, C. (2006). Coordinated cell-shape changes control epithelial movement in zebrafish and *Drosophila*. *Development* **133**, 2671-2681.
Li, W., Herman, R. K. and Shaw, J. E. (1992). Analysis of the *Caenorhabditis elegans* axonal guidance and outgrowth gene *unc-33*. *Genetics* **132**, 675-689.
Machida, N., Umikawa, M., Takei, K., Sakima, N., Myagmar, B. E., Taira, K., Uezato, H., Ogawa, Y. and Kariya, K. (2004). Mitogen-activated protein kinase kinase kinase kinase 4 as a putative effector of Rap2 to activate the c-Jun N-terminal kinase. *J. Biol. Chem.* **279**, 15711-15714.
McIntire, S. L., Garriga, G., White, J., Jacobson, D. and Horvitz, H. R. (1992). Genes necessary for directed axonal elongation or fasciculation in *C. elegans*. *Neuron* **8**, 307-322.
Mizuno, T., Hisamoto, N., Terada, T., Kondo, T., Adachi, M., Nishida, E., Kim, D. H., Ausubel, F. M. and Matsumoto, K. (2004). The *Caenorhabditis elegans* MAPK phosphatase VHP-1 mediates a novel JNK-like signaling pathway in stress response. *EMBO J.* **23**, 2226-2234.
Norris, A. D., Dyer, J. O. and Lundquist, E. A. (2009). The Arp2/3 complex, UNC-115/abLIM, and UNC-34/Enabled regulate axon guidance and growth cone filopodia formation in *Caenorhabditis elegans*. *Neural Dev.* **4**, 38.
Paricio, N., Feiguin, F., Boutros, M., Eaton, S. and Mlodzik, M. (1999). The *Drosophila* STE20-like kinase misshapen is required downstream of the Frizzled receptor in planar polarity signalling. *EMBO J.* **18**, 4669-4678.
Petrie, R. J., Doyle, A. D. and Yamada, K. M. (2009). Random versus directionally persistent cell migration. *Nat. Rev. Mol. Cell Biol.* **10**, 538-549.
Poinat, P., De Arcangelis, A., Sookhareea, S., Zhu, X., Hedgecock, E. M., Labouesse, M. and Georges-Labouesse, E. (2002). A conserved interaction between beta1 integrin/PAT-3 and Nck-interacting kinase/MIG-15 that mediates commissural axon navigation in *C. elegans*. *Curr. Biol.* **12**, 622-631.
Quinn, C. C. and Wadsworth, W. G. (2008). Axon guidance: asymmetric signalling orients polarized outgrowth. *Trends Cell Biol.* **18**, 597-603.
Quinn, C. C., Pfeil, D. S., Chen, E., Stovall, E. L., Harden, M. V., Gavin, M. K., Forrester, W. C., Ryder, E. F., Soto, M. C. and Wadsworth, W. G. (2006). UNC-6/netrin and SLT-1/slit guidance cues orient axon outgrowth mediated by MIG-10/RIAM/lamellipodin. *Curr. Biol.* **16**, 845-853.
Quinn, C. C., Pfeil, D. S. and Wadsworth, W. G. (2008). CED-10/Rac1 mediates axon guidance by regulating the asymmetric distribution of MIG-10/lamellipodin. *Curr. Biol.* **18**, 808-813.
Ramesh, V. (2004). Merlin and the ERM proteins in Schwann cells, neurons and growth cones. *Nat. Rev. Neurosci.* **5**, 462-470.
Schmitz, C., Kinge, P. and Hutter, H. (2007). Axon guidance genes identified in a large-scale RNAi screen using the RNAi-hypersensitive *Caenorhabditis elegans* strain *nre-1(hd20) lin-15b(hd126)*. *Proc. Natl. Acad. Sci. USA* **104**, 834-839.
Shakir, M. A., Gill, J. S. and Lundquist, E. A. (2006). Interactions of UNC-34 Enabled with Rac GTPases and the NIK kinase MIG-15 in *Caenorhabditis elegans* axon pathfinding and neuronal migration. *Genetics* **172**, 893-913.
Silhankova, M. and Korswagen, H. C. (2007). Migration of neuronal cells along the anterior-posterior body axis of *C. elegans*: Wnts are in control. *Curr. Opin. Genet. Dev.* **17**, 320-325.
Simmer, F., Moorman, C., van der Linden, A. M., Kuijk, E., van den Berghe, P. V. E., Kamath, R. S., Fraser, A. G., Ahringer, J. and Plasterk, R. H. A. (2003). Genome-wide RNAi of *C. elegans* using the hypersensitive *rrf-3* strain reveals novel gene functions. *PLoS Biol.* **1**, E12.
Stringham, E. E., Pujol, N., Vanderkerckove, J. and Bogaert, T. (2002). *unc-53* controls longitudinal migration in *C. elegans*. *Development* **129**, 3367-3379.
Su, Y. C., Treisman, J. E. and Skolnik, E. Y. (1998). The *Drosophila* Ste20-related kinase misshapen is required for embryonic dorsal closure and acts through a JNK MAPK module on an evolutionarily conserved signalling pathway. *Genes Dev.* **12**, 2371-2380.
Sulston, J. E. and Horvitz, H. R. (1977). Post-embryonic cell lineages of the nematode, *Caenorhabditis elegans*. *Dev. Biol.* **56**, 110-156.
Sulston, J. E., Schierenberg, E., White, J. G. and Thomson, J. N. (1983). The embryonic cell lineage of the nematode *Caenorhabditis elegans*. *Dev. Biol.* **100**, 64-119.
Tahirovic, S., Hellal, F., Neukirchen, D., Hindges, R., Garvalov, B. K., Flynn, K. C., Stradal, T. E., Chrostek-Grashoff, A., Brakebusch, C. and Bradke, F. (2010). Rac1 regulates neuronal polarization through the WAVE complex. *J. Neurosci.* **30**, 6930-6943.
Timmons, L., Court, D. L. and Fire, A. (2001). Ingestion of bacterially expressed dsRNAs can produce specific and potent genetic interference in *Caenorhabditis elegans*. *Gene* **263**, 103-112.
Van Fürden, D., Johnson, K., Segbert, C. and Bossinger, O. (2004). The *C. elegans* ezrin-radixin-moesin protein ERM-1 is necessary for apical junction remodelling and tubulogenesis in the intestine. *Dev. Biol.* **272**, 262-276.
Withee, J., Galligan, B., Hawkins, N. and Garriga, G. (2004). *Caenorhabditis elegans* WASP and Ena/VASP proteins play compensatory roles in morphogenesis and neuronal cell migration. *Genetics* **167**, 1165-1176.
Xue, Y., Wang, X., Li, Z., Gotoh, N., Chapman, D. and Skolnik, E. Y. (2001). Mesodermal patterning defect in mice lacking the Ste20 NCK interacting kinase (NIK). *Development* **128**, 1559-1572.
Zhong, W. and Sternberg, P. W. (2006). Genome-wide prediction of *C. elegans* genetic interactions. *Science* **311**, 1481-1484.

Table S1. List of primers for all genes tested in the *mig_15* enhancer screen

Sequence	Gene name	Ggenomic position (bp)	Primers
B0205.4	*B0205.4*	I:10744432..10741426	sji_B0205.4
B0350.2	*unc-44*	IV:5966640..6004843	sji_B0350.2
B0393.1	*rps-0*	III:4754047..4752962	sji_B0393.1
C01G6.8	*cam-1*	II:9310226..9295842	sji_C01G6.8
C01G8.5	*erm-1*	I:5291608..5284065	sji_C01G8.5
C02B4.1	*adt-1*	X:12678751..12689198	sji_C02B4.1
C02F4.1	*ced-5*	IV:10484082..10492924	sji_C02F4.1
C02F5.1	*knl-1*	III:8250551..8254237	sji_C02F5.1
C04A11.3	*gck-4*	X:13677181..13681999	sji_C04A11.3
C04A11.4	*adm-2*	X:13687894..13695694	sji_C04A11.4
C04F6.4	*unc-78*	X:3411671..3408662	sji_C04F6.4
C04G6.1	*mpk-2*	II:5104101..5108855	sji_C04G6.1
C05D2.1	*daf-4*	III:5624968..5632374	sji_C05D2.1
C06C3.3	*C06C3.3*	II:9372285..9369092	sji_C06C3.3
C07A9.5	*C07A9.5*	III:9682725..9681420	sji_C07A9.5
C07G1.4	*wsp-1*	IV:8198932..8188888	sji_C07G1.4
C09B8.7	*pak-1*	X:6048570..6044269	sji_C09B8.7
C09D8.1	*ptp-3*	II:10975461..11012163	sji_C09D8.1
C10H11.1	*viln-1*	I:4747628..4759602	sji_C10H11.1
C10H11.9	*let-502(sb118)*	I:4744322..4738171	-
C10H11.9	*let-502*	I:4744322..4738171	sji_C10H11.9
C12C8.3	*lin-41*	I:9342486..9334793	sji_C12C8.3
C14F11.2	*C14F11.2*	X:6213869..6208724	sji_C14F11.2
C23F12.1	*flna-1*	X:9412607..9426614	sji_C23F12.1
C23F12.2	*flnb-1*	X:9397683..9407992	sji_C23F12.2
C24A11.8	*frm-4*	I:5408347..5402898	sji_C24A11.2
C26C6.2	*goa-1*	I:7522112..7526710	sji_C26C6.2
C26D10.5	*eff-1*	II:8346622..8350481	sji_C26D10.5
C29F9.7	*pat-4*	III:94808..89460	sji_C29F9.7
C34B4.1	*max-1*	V:13110145..13098719	sji_C34B4.1
C36B1.1	*cle-1*	I:8724272..8705680	sji_F39H11.4
C37A2.4	*cye-1*	I:6780807..6784360	sji_C37A2.4
C37A5.9	*pry-1*	I:14179347..14172827	sji_C37A5.10
C37A5.9	*pry-1*	I:14179347..14172827	sji_C37A5.9
C38C3.5	*unc-60*	V:1474915..1476608	reconstructed
C41G7.5	*ahr-1*	I:9522569..9531119	sji_C41G7.5
C43E11.6	*nab-1*	I:4229578..4236043	sji_C43E11.6
C43G2.2	*bicd-1*	IV:6572312..6565884	sji_C43G2.2
C45B11.1	*pak-2*	V:11039400..11036443	sji_C45B11.1
C45G3.1	*aspm-1*	I:9226377..9221835	sji_C45G3.1
C46G7.4	*pqn-22*	IV:6034522..6019688	sji_C46G7.4
C46H11.11	*fhod-1*	I:5061927..5058623	sji_C46H11.11
C47E8.7	*unc-112*	V:14696911..14691826	sji_C47E8.7
C52E12.2	*unc-104(e1265)*	II:6994990..7010563	-
C53D6.2	*unc-129*	IV:9005390..9002817	sji_C53D6.2
C54D1.5	*lam-2*	X:7151092..7143870	sji_C54D1.5
C56E6.4	*C56E6.4*	II:6528522..6526778	sji_C56E6.4
D1069.2	*cpn-2*	II:337338..339247	sji_D1069.2
E03G2.3	*mec-5*	X:15943929..15948873	sji_E03G2.3
EGAP1.3	*zmp-1*	III:5932904..5926849	sji_C28H8.1
F02A9.6	*glo-1*	III:9092152..9099594	sji_F02A9.6
F08B1.1	*vhp-1*	II:5322980..5340791	sji_F08B1.1
F08F1.8	*ttb-1*	X:8423671..8422417	sji_F08F1.8
F09B9.2	*unc-115*	X:10146825..10153073	sji_F09B9.2
F09B9.2	*unc-115*	X:10146825..10153073	sji_F09B9.2
F09C3.1	*pes-7*	I:14263285..14271296	sji_F09C3.1
F09C6.1	*F09C6.1*	V:16888278..16887212	sji_F09C6.1
F09F7.5	*F09F7.5*	III:5547024..5551158	sji_F09F7.5
F10E9.6	*mig-10*	III:8279028..8305755	sji_F10E9.6
F11H8.4	*cyk-1*	III:7029125..7023571	sji_F11H8.4
F14D12.2	*unc-97*	X:5593094..5594926	sji_F14D12.2
F15B9.4	*inft-2*	V:13002151..13006778	reconstructed
F15D3.1	*dys-1*	I:11557780..11527065	sji_F15D3.10
F18H3.5	*cdk-4*	X:13518825..13515972	sji_F18H3.5
F22B5.1	*evl-20*	II:8444231..8445029	sji_F22B5.1
F22B5.7	*zyg-9*	II:8457742..8464441	sji_F22B5.7
F25B3.1	*ehbp-1*	V:9550445..9555830	sji_F25B3.1
F25H8.3	*ggn-1*	IV:9945747..9935039	sji_F25H8.3
F26E4.8	*tba-1(or346)*	I:9787389..9785768	-
F26F4.5	*F26F4.5*	III:4891213..4887882	sji_F26F4.5
F28H1.2	*cpn-3*	I:3987893..3988698	sji_F28H1.2
F31B12.3	*frm-9*	X:10818641..10816679	sji_F31B12.3
F33E2.2	*dlk-1*	I:12572790..12565793	sji_F33E2.2
F35B3.5	*pqn-34*	X:17030133..17021735	sji_F35B3.5
F35C8.6	*pfn-2*	X:5354109..5353068	sji_F35C8.6
F38A6.2	*elp-1*	V:20765431..20760225	sji_F38A6.2
F38E9.5	*F38E9.5*	X:16446116..16451251	sji_F38E9.5
F39D8.3	*F39D8.3*	X:15422412..15424737	sji_F39D8.3
F39G3.8	*tig-2*	V:4730155..4726715	sji_F39G3.8
F40E10.1	*hch-1*	X:14699897..14696332	sji_F40E10.1
F41C6.1	*unc-6*	X:6889643..6897094	sji_F41C6.1
F42A10.2	*nfm-1*	III:6159783..6164514	sji_F42A10.2
F42G8.3	*pmk-2*	IV:8143481..8148621	sji_F42G8.3
F42G8.4	*pmk-3*	IV:8139200..8143118	sji_F42G8.4
F42G9.9	*pti-1*	III:763805..771377	sji_F42G9.9
F43C1.2	*mpk-1*	III:4228066..4216742	sji_F43C1.2
F43G9.9	*cpn-1*	I:8637931..8636122	sji_F43G9.9
F45E10.1	*unc-53*	II:11089371..11058016	sji_F45E10.1
F45E12.2	*brf-1*	II:7305794..7308613	sji_F45E12.2
F46B6.5	*F46B6.5*	V:9782862..9779350	sji_F46B6.5
F46C3.3	*hum-4*	X:11433447..11420414	sji_F46C3.3
F47D12.4	*hmg-1.2*	III:6280328..6282361	sji_F47D12.4
F49B2.5	*src-2*	I:14322224..14328913	sji_F49B2.5
F49B2.5	*kin-22*	I:14322224..14328913	sji_F49B2.5
F49D11.8	*cpn-4*	I:10925737..10924331	sji_F49D11.8
F53E2.1	*taq-304*	V:1467573..1470931	sji_F53E2.1
F54F2.1	*pat-2*	III:8818809..8825177	sji_F54F2.1
F54F3.1	*nid-1*	V:12910092..12917169	sji_F54F3.1
F55C7.7	*unc-73*	I:4031628..3999350	sji_F55C7.7
F56D12.4	*lip-1*	II:1327001..1350142	sji_F56D12.2
F56D12.4	*lip-1*	II:1327001..1350142	sji_F56D12.3
F56H11.1	*fbl-1*	IV:9540783..9546227	sji_F56H11.1
F57B7.4	*mig-17*	V:11446629..11449222	sji_F57B7.4
F58A3.2	*eql-15*	X:11016336..11023321	sji_F58A3.2
F58B6.2	*inft-1*	III:1103212..1111911	sji_F58B6.2
F59A6.1	*nsy-1*	II:5022748..5029967	sji_F59A6.1
F59A6.5	*F59A6.5*	II:4999510..5003779	sji_F59A6.5
F59F3.1	*ver-3*	X:10992436..10997755	sji_F59F3.1
F59F5.6	*syd-2*	X:10555169..10549053	sji_F59F5.6
H05G16.1	*frm-3*	X:11576177..11581648	sji_H05G16.1
H09G03.2	*frm-8*	III:3219141..3200789	sji_H09G03.2
H24G06.1	*H24G06.1*	V:9446146..9460608	sji_F07D3.1
H39E23.1	*par-1*	V:14141097..14112017	sji_H39E23.1
K01B6.1	*fozi-1*	III:9285951..9296528	sji_K01B6.1
K03E6.6	*pfn-3*	X:1080622..1079489	sji_K03E6.6
K04G2.8	*apr-1*	I:8050037..8055460	sji_K04G2.8
K06A4.3	*gsnl-1*	V:9496381..9499169	sji_K06A4.3
K06A5.8	*K06A5.8*	I:6488948..6476755	sji_K06A5.8
K08B12.5	*mrck-1*	V:6267174..6257375	sji_K08B12.1
K08C7.3	*epi-1*	IV:10666799..10679261	sji_K08C7.3
K08E3.4	*K08E3.4*	III:13761585..13758804	sji_K08E3.4
K11C4.3	*unc-70*	V:6881154..6892034	sji_K11C4.3
K12F2.2	*vab-8*	V:12213304..12225897	sji_K12F2.2
M03D4.1	*zen-4*	IV:6118208..6121745	sji_M03D4.1
M04F3.4	*M04F3.4*	I:4773025..4771842	sji_M04F3.4
M116.5	*M116.5*	IV:8420990..8414275	sji_M116.5
R05D3.7	*unc-116*	III:8355093..8351168	sji_R05D3.7
R06C1.3	*wve-1*	I:11929495..11925263	sji_R06C1.3
R07G3.1	*cdc-42(gk388)*	II:7616383..7618167	-
R07H5.2	*R07H5.2*	IV:11179615..11182972	sji_R07H5.2
R107.6	*cls-2*	III:9054957..9058787	sji_R107.6
R107.8	*lin-12*	III:9071299..9060153	sji_R107.8
R148.2	*R148.2*	III:3183682..3184991	sji_R148.2
R31.1	*sma-1*	V:11901156..11916429	sji_R31.1
R53.3	*egl-43*	II:9955107..9962905	sji_R53.3
T03F6.5	*lis-1*	III:13376226..13370691	sji_T03F6.5
T04C9.6	*frm-2*	III:5982069..5976735	sji_T04C9.6
T07A9.3	*kgb-1*	IV:410026..405683	sji_T07A9.3
T10H10.1	*hum-6*	X:2303114..2314903	sji_T10H10.1
T11B7.4	*gtp-2*	IV:8852482..8862209	sji_T11B7.4
T16G12.1	*T16G12.1*	III:10049670..10040080	sji_T16G12.1
T21D12.4	*pat-6*	IV:264232..261899	sji_T21D12.4
T21H8.1	*T21H8.1*	X:13873280..13864961	sji_T21H8.1
T23G5.3	*T23G5.3*	III:9231118..9229143	sji_T23G5.3
T24B8.4	*T24B8.4*	II:9071491..9064961	sji_T24B8.4
T24H10.7	*jun-1*	II:9113138..9132129	sji_T24H10.2
T26E3.3	*par-6*	I:12669369..12674436	sji_T26E3.3
T27E9.3	*cdk-5*	III:13466270..13464567	sji_T27E9.3
VW02B12L.3	*ebp-2*	II:11442630..11443908	sji_VW02B12L.3
W03F11.6	*afd-1*	I:2160044..2209630	sji_Y39G10A_236.c
W04D2.1	*atn-1*	V:12478219..12484254	sji_W04D2.1
W04H10.3	*nhl-3*	II:602126..595209	sji_W04H10.3
W06F12.1	*lit-1*	III:13701873..13724281	sji_W06F12.1
W07G1.5	*W07G1.5*	II:13962311..13959133	sji_W07G1.5
Y105E8A.6	*unc-95*	I:14384724..14381367	sji_Y105E8C.s
Y18D10A.20	*pfn-1*	I:12921988..12923521	sji_Y18D10A.20
Y34D9A.4	*spd-1*	I:1033438..1030635	sji_Y34D9A.151.d
Y37D8A.13	*unc-71*	III:12891618..12880918	sji_Y37D8A.13
Y37E11C.1	*unc-33*	IV:3516818..3526598	sji_Y37E11C.1
Y38F1A.10	*max-2*	II:13025746..13014240	sji_Y38F1A.10
Y39H10A.7	*chk-1*	V:3759283..3756825	sji_Y39H10A_224.a
Y41D4B.13	*ced-2*	IV:1597314..1601619	sji_Y41D4A_3457.c
Y48C3A.9	*Y48C3A.9*	II:13330680..13325788	sji_Y48C3A.k
Y48G9A.4	*frl-1*	III:2134463..2151527	reconstructed
Y50D4C.1	*unc-34*	V:982536..995406	(Fleming et al., 2010)
Y50D7A.10	*Y50D7A.10*	III:315457..322080	reconstructed
Y54E2A.3	*tac-1*	II:14753772..14752781	sji_Y54E2A.3
Y59A8B.23	*gck-3*	V:17966814..17954088	sji_Y59A8A.b
Y66H1B.2	*Y66H1B.2*	IV:364340..359584	sji_Y66H1B.2
Y66H1B.3	*Y66H1B.3*	IV:376064..370293	sji_Y66H1B.3
Y73B6A.5	*lin-45*	IV:6748408..6742522	sji_Y73B6A.a
ZC101.2	*unc-52*	II:14666846..14647267	sji_ZC101.2
ZC404.9	*gck-2*	V:6792648..6788433	sji_ZC404.9
ZC416.4	*kgb-2*	IV:3806791..3609114	sji_ZC416.4
ZC416.6	*ZC416.6*	IV:3613067..3609226	sji_ZC416.6
ZK1098.10	*unc-16(e109)*	III:9546159..9556413	-
ZK1151.1	*vab-10*	I:11792106..11764283	sji_ZK1151.1
ZK1321.4	*ZK1321.4*	II:9773797..9770682	sji_ZK1321.4
ZK270.2	*frm-1*	I:14900197..14875748	sji_ZK270.2
ZK370.3	*ZK370.3*	III:8720103..8725236	sji_ZK370.3
ZK377.2	*sax-3*	X:3465913..3451933	sji_ZK377.2
ZK470.5	*nck-1*	X:4153419..4148633	sji_ZK470.5
ZK637.8	*unc-32*	III:8905525..8911657	sji_ZK637.8
ZK783.4	*flt-1*	III:7655960..7650495	sji_ZK783.4
ZK973.6	*anc-1*	I:4321096..4359081	sji_ZK973.f

Table S2. List of *mig-15* enhancers identified in the screen

Gene	Description	Inactivation in *mig-15(rh148)* background†	Inactivation in wild-type background†	References
Actin-binding proteins				
***mig-15(rh148)* enhancers**				
unc-70	beta-spectrin ortholog	+	–	(Hammarlund et al., 2000 ; Hammarlund et al., 2007)
*pfn-2**	profilin ortholog	+	–	
*F38E9.5**	twinfilin ortholog	+	–	
erm-1	ezrin-radixin-moesin	+	–	(Norris et al., 2009)
unc-115	AbLim ortholog	++	–	(Lundquist et al., 1998)
*pfn-1**	profilin ortholog	+/–	–	
*pqn-34**	prion-like-(Q/N-rich)-domain-bearing protein	+/–	–	
*frm-1**	FERM domain protein	+/–	–	
max-1	PH/MyTH4/FERM domain-containing protein	++	–	(Huang et al., 2002)
***mig-15*-independent enhancers**				
wve-1	WAVE ortholog	++	++	(Withee et al., 2004)
unc-53	NAV1, NAV2/RAINB1, NAV3 ortholog	++	+/–	(Hekimi and Kershaw, 1993)
unc-73	trio ortholog	++	++	(Wu et al., 2002 ; Lundquist et al., 2001)
*aspm-1**	abnormal spindle ortholog	+	+	
*vab-10**	plectin ortholog	+	++	
wsp-1	WASP ortholog	+	+	(Withee et al., 2004)
*cpn-4**	calponin ortholog	+/–	+/–	
*sma-1**	beta-H spectrin ortholog	+/–	+/–	
ced-2	CrkII ortholog	+/–	+/–	(Wu et al., 2002)
unc-34	Ena/VASP ortholog	++	+	(Shakir et al., 2006; Fleming et al., 2010)
Microtubule-binding proteins				
***mig-15(rh148)* enhancers**				
*bicd-1**	bicaudal-D ortholog	+	–	
tba-1(or346)	alpha tubulin ortholog	+	–	(Baran et al., 2010)
unc-33	CRMP2 ortholog	+	–	(Li et al., 1992 ; Tsuboi et al., 2005)
unc-116	kinesin 1 heavy chain/KIF5 ortholog	+	–	(Schmitz et al., 2007)
*tac-1**	transforming acidic coiled-coil-containing protein ortholog	+/–	–	
Extracellular matrix proteins				
***mig-15(rh148)* enhancers**				
cle-1	collagen XVIII ortholog	+	–	(Ackley et al., 2001)
***mig-15*-independent enhancers**				
epi-1	laminin alpha chain ortholog	++	++	(Zhu et al., 1999)
Signaling proteins				
***mig-15(rh148)* enhancers**				
*evl-20**	ARL2 ortholog	+	–	
*let-502(sb118)**	Rho Kinase ortholog	+P	–	
mig-10	lamellipodin ortholog	+	–	(Quinn et al., 2006 ; Chang et al., 2006 ; Adler et al., 2006)
unc-6	netrin ortholog	+	–	(Hedgecock et al., 1990)
*unc-16(e109)**	JIP3/JSAP1 ortholog	+	–	
ahr-1	aryl Hydrocarbon Receptor ortholog	+/–	–	(Qin and Powell-Coffman, 2004)
*alp-1**	adaptor protein Enigma ortholog	+/–	–	
cam-1	ROR receptor tyrosine kinase ortholog	+/–	–	(Forrester et al., 1999)
ced-5	DOCK180 ortholog	+/–	–	(Wu et al., 2002 ; Lundquist et al., 2001)
*kgb-1**	JNK MAP Kinase ortholog	+/–	–	
*pmk-2**	p38 MAP Kinase ortholog	+/–	–	
pry-1	axin ortholog	+/–	–	(Schmitz et al., 2007)
unc-129	TGF beta-like	+/–	–	(Colavita et al., 1998)

***mig-15*-independent enhancers**				
*cdc-42(gk388)**	Cdc42 ortholog	+	+/–	
unc-71	ADAM-type metalloprotease	+	++	(Huang et al., 2003)
*chk-1**	checkpoint kinase ortholog	+/–	+/–	
*ver-3**	VEGF receptor ortholog	+/–	+	
Myosins				
***mig-15(rh148)* enhancers**				
*hum-6**	myosin VIIA ortholog	+	–	
Transcription factors				
***mig-15(rh148)* enhancers**				
egl-43	zinc finger protein	+/–	–	(Garriga et al., 1993)
Unknown function				
***mig-15*-independent enhancers**				
*C56E6.4**	doublecortin domain	+/–	+	
*F09C6.1**	no known domains	+/–	+/–	

*Gene not previously implicated in *C. elegans* neuronal development.
†The identified *mig-15* enhancers were classified according to the function assigned to the protein they encode. RNAi results shown for the *mig-15(rh148)* genetic background sum up the results obtained with *rrf-3(pk1426); mig-15(rh148) oxIs12* and *eri-1(mg366); mig-15(rh148) oxIs12* animals. Results shown for the wild-type genetic background sum up together the results obtained with *rrf-3(pk1426); oxIs12* and *eri-1(mg366); oxIs12* animals. Positive controls for RNAi efficiency were bacterial clones targeting GFP and axon guidance regulators. Negative controls were clones targeting the *lacZ* bacterial gene.
–, no difference compared with negative controls; +/–, <20% of the worms showed at least 100% enhancement (*mig-15* background) or commissure defects (wild-type background); +, >20% of the worms showed 100% enhancement (weak enhancers, *mig-15* background) or commissure defects (wild-type background); ++, >20% of the worms showed : more than 100% enhancement (strong enhancers, *mig-15* background) / commissure defects (wild-type background); P, P-cell migration defects (VD neurons cell bodies lateral).

Additional references

Ackley, B. D., Crew, J. R., Elamaa, H., Pihlajaniemi, T., Kuo, C. J. and Kramer, J. M. (2001). The NC1/endostatin domain of *Caenorhabditis elegans* type XVIII collagen affects cell migration and axon guidance. *J. Cell Biol.* **152**, 1219-1232.

Baran, R., Castelblanco, L., Tang, G., Shapiro, I., Goncharov, A. and Jin, Y. (2010). Motor neuron synapse and axon defects in a *C. elegans* Alpha-Tubulin mutant. *PLoS One* **5**, e9655.

Colavita, A., Krishna, S., Zheng, H., Padgett, R. W. and Culotti, J. G. (1998). Pioneer axon guidance by UNC-129, a *C. elegans* TGF-beta. *Science* **281**, 706-709.

Forrester, W. C., Dell, M., Perens, E. and Garriga, G. (1999). A *C. elegans* Ror receptor tyrosine kinase regulates cell motility and asymmetric cell division. *Nature* **400**, 881-885.

Garriga, G., Guenther, C. and Horvitz, H. R. (1993). Migrations of the *Caenorhabditis elegans* HSNs are regulated by *egl-43*, a gene encoding two zinc finger proteins. *Genes Dev.* **7**, 2097-2109.

Hammarlund, M., Davis, W. S. and Jorgensen, E. M. (2000). Mutations in beta-spectrin disrupt axon outgrowth and sarcomere structure. *J. Cell Biol.* **149**, 931-942.

Hedgecock, E. M., Culotti, J. G. and Hall, D. H. (1990). The *unc-5*, *unc-6*, and *unc-40* genes guide circumferential migrations of pioneer axons and mesodermal cells on the epidermis in *C. elegans*. *Neuron* **4**, 61-85.

Hekimi, S. and Kershaw, D. (1993). Axonal guidance defects in a *Caenorhabditis elegans* mutant reveal cell-extrinsic determinants of neuronal morphology. *J. Neurosci.* **13**, 4254-4271.

Huang, X., Cheng, H. J., Tessier-Lavigne, M. and Jin, Y. (2002). MAX-1, a novel PH/MyTH4/FERM domain cytoplasmic protein implicated in netrin-mediated axon repulsion. *Neuron* **34**, 563-576.

Huang, X., Huang, P., Robinson, M. K., Stern, M. J. and Jin, Y. (2003). UNC-71, a disintegrin and metalloprotease (ADAM) protein, regulates motor axon guidance and sex myoblast migration in *C. elegans*. *Development* **130**, 3147-3161.

Lundquist, E. A., Herman, R. K., Shaw, J. E. and Bargmann, C. I. (1998). UNC-115, a conserved protein with predicted LIM and actin-binding domains, mediates axon guidance in *C. elegans*. *Neuron* **21**, 385-392.

Lundquist, E. A., Reddien, P. W., Hartwieg, E., Horvitz, H. R. and Bargmann, C. I. (2001). Three *C. elegans* Rac proteins and several alternative Rac regulators control axon guidance, cell migration and apoptotic cell phagocytosis. *Development* **128**, 4475-4488.

Qin, H. and Powell-Coffman, J. A. (2004). The *Caenorhabditis elegans* aryl hydrocarbon receptor, AHR-1, regulates neuronal development. *Dev. Biol.* **270**, 64-75.

Tsuboi, D., Hikita, T., Qadota, H., Amano, M. and Kaibuchi, K. (2005). Regulatory machinery of UNC-33 Ce-CRMP localization in neurites during neuronal development in *Caenorhabditis elegans*. *J. Neurochem.* **95**, 1629-1641.

Wu, Y., Cheng, T., Lee, M. and Weng, N. (2002). Distinct rac activation pathways control *Caenorhabditis elegans* cell migration and axon outgrowth. *Dev. Biol.* **250**, 145-155.

Zhu, X., Joh, K., Hedgecock, E. M. and Hori, K. (1999). Identification of *epi-1* locus as a laminin alpha chain gene in the nematode *Caenorhabditis elegans* and characterization of epi-1 mutant alleles. *DNA Seq.* **10**, 207-217.